Pushing the Fano limit

Improvement of Fano-limited single-photon counting MKID detectors

Aaron Dantuma

Delft University of Technology

TU Delft

Pushing the Fano limit

Improvement of Fano-limited single-photon counting MKID detectors

by

Aaron Dantuma

to obtain the degree of Bachelor of Science

at the Delft University of Technology.

Student number:	5410916	
Project duration:	October 16, 2023 – January 19, 2024	
Thesis committee:	Dr. ir. P. J. de Visser,	SRON Leiden, supervisor
	Ir. S. A. H. de Rooij,	TU Delft, supervisor
	Prof. dr. ir. J. J. A. Baselmans,	TU Delft, SRON Leiden
	Prof. dr. Yaroslav Blanter,	TU Delft

Cover:	Artist impression of WASP-39 b and its star. The presence of carbon dioxide in WASP-39 b's atmosphere was discovered by NASA's James Webb telescope. Image by NASA, ESA, CSA, and J. Olmsted [1].
Style:	TU Delft Report Style, with modifications by Daan Zwaneveld

TU Delft

Preface

This report was written to obtain the degree of Bachelor of Science at the faculty Applied Sciences at the Delft University of Technology. The project was carried out in the Experimental Astronomy group, at the faculty of Mathematics, Electrical Engineering and Computer Science.

I would like to thank my supervisor Pieter de Visser and Steven de Rooij for their unrelenting support throughout this project and for being the ideal sparring partners to discuss questions and ideas with, along with the other members of the Terahertz Sensing group who have shared their insights with me. I would also like to thank my friends and family for putting up with my rambling about probability distributions, phonon interactions and Fano factors, trying to make sense of what I was saying.

Abstract

Single-photon counting MKIDs (microwave kinetic inductance detectors) are light detectors that use the change in the electric properties of a superconductor due to electron excitations to detect individual photons. Novel MKIDs are limited by an uncertainty in the down-conversion process from a photon to a number of excited electrons, called the Fano factor. These Fano-limited MKIDs could be improved if a method is found to lower the Fano factor, further increasing the resolving power of MKIDs, and possibly other detectors that rely on pair-breaking. In this report, a Monte Carlo simulation is constructed to simulate a large number of individual photons incident on a superconductor. The data from the simulation is then used to calculate the Fano factor. Simulations are performed to test the dependence of the Fano factor on both the choice of superconducting material (Sn, Nb and Al), and the energy of the photon incident on the superconductor. $F = 0.208 \pm 0.003$ is found independent of material and photon energy. The dependency of the Fano factor on the phonon spectrum of the superconductor is tested and the possible implementation of phonon spectrum tuning in order to improve the Fano factor are discussed. We find that F can be reduced to $F = 0.151 \pm 0.003$ by implementing a phonon band gap from 0-2Δ. The resolving power of an MKID then improves with up to 24%. To realise this band gap, holes could be introduced in the superconductor, creating a pattern with a period of approximately 80 nm. The smallest feature size in this pattern would be approximately 40 nm, which is achievable with current technology. It is unlikely that a perfect 0-2Δ band gap can be created and the real improvement of F by implementation of a phonon band gap would probably be lower than 24%. We conclude that improvement of the resolving power of an MKID via the Fano factor is possible in theory, but further research is required to test the viability of such a band gap and calculate the specific shape and size of these holes.

Contents

1

Introduction

Astronomy is a discipline as old as mankind itself. Our ancestors used their eyes to peer into the night sky to discover constellations, along with the planets in our solar system. Later on, instruments like the telescope made it easier to study the stars. Nowadays, scientists are pushing technology to perform more accurate measurements over longer and longer distances. An example of recent advancements is NASA's James Webb Space Telescope, the 10 billion USD space telescope that launched in 2021 [2]. One discipline in astronomy is exoplanet spectroscopy [3], used for the identification of molecules present in the atmospheres of distant planets. Because the light coming from an exoplanet is 10^{10} times less intense than the light from the star it orbits, very sensitive photon detectors with wide bandwidths are required [4]. The sensitivity of optical instruments can be measured with the resolving power of the instrument. The resolving power is a dimensionless quantity that characterizes the extent to which a detector can distinguish different wavelengths of light from each other. For exoplanet spectroscopy, a detector with zero noise and a resolving power of 100 to 150 is needed [4].
A single-photon counting MKID (microwave kinetic inductance detector) is a microscopic detector that uses the properties of superconducting metals to detect individual photons in the visible to near-infrared wavelength range [5]. A photon that is absorbed by the detector causes electron excitations, temporarily shifting the electrical properties of a superconducting inductor. This temporary shift can be measured via the readout line of the chip. A big advantage of this type of detector, compared to other superconducting detectors, is that it can be used in large arrays [6]. The resolving power of novel MKIDs is limited by an uncertainty in the number of electrons that are excited by an incoming photon [4]. The quantity that describes the spread in the number of excited electrons is called the Fano factor, which is generally considered a fundamental limit in the resolving power of MKIDs. But how fundamental is this Fano limit really? Can MKID detectors be engineered in a way that circumvents this limiting factor and improve Fano-limited MKIDs? The results found in this study may not only be applied to single-photon counting MKIDs, but also to other detectors that rely on Cooper pair breaking.
In this report, after providing some theoretical background on phonons, superconductivity and MKID detectors (chapter 2), a Monte Carlo simulation is created to simulate the processes that take place in an MKID (chapter 3). The data from the simulation is used to calculate the Fano factor. After this has been accomplished, different experiments are performed to find factors that may influence the Fano factor and the results are discussed (chapter 4). The main research question of this report is:

To what extent can the Fano factor be improved to enhance the resolving power of single-photon counting MKIDs?

This question can be answered by either proving that the Fano factor depends on certain factors like material properties, or by proving that the Fano factor can not be influenced by the input parameters of the simulation. In the first case the resolving power of MKIDs may be improved further by the implementation of the found solutions. In the latter case, the resolving power of MKIDs should be improved in other ways rather than improving the Fano factor.

2

Theoretical background

Before we can construct a simulation to calculate the Fano factor, we need to understand some things about MKIDs. This chapter will introduce the necessary concepts that need to be understood to set up the simulation and calculate the Fano factor in an MKID. Phonons (2.1), superconductivity (2.2) and a more detailed explanation of MKIDs (2.3) are discussed, which enables us to understand what the Fano factor is and why it is important in MKID measurements (2.5).

2.1. Phonons

Solid state physics includes the study of the crystal structures of materials. These crystal structures, or lattices, consist of a network of atoms which can carry vibrations and may consist of more than one type of atom (e.g. salts). To effectively describe them, crystal structures are often interpreted as point masses connected by springs. As mentioned before, these systems allow a range of oscillations, called lattice vibrations. To conveniently describe these vibrations, the concept of phonons is used. The energy of a phonon is, analogous to the energy of photons, quantified into a packet of energy $\Omega = \hbar\omega$, where ω is the angular frequency of the lattice vibration mode and $\hbar$ the reduced Planck constant. It is important to note that the maximum energy of a phonon is capped by the maximum phonon frequency $\hbar\omega_{max}$. This maximum frequency exists because the shortest wavelength a lattice vibration can have is half the distance between atoms in the lattice. At this wavelength, neighbouring atoms have a phase difference of π and since $\omega = 2\pi\lambda/v$, the maximum frequency ω_{max} is reached. Therefore the maximum energy of a photon is given by $\hbar\omega_{max}$. $\hbar\omega_{max}$ is often approximated with the Debye energy $\hbar\omega_D$, with ω_D the Debye frequency, or the approximated maximum angular frequency at which a crystal lattice can vibrate [7]. Because different materials allow different phonon modes, the phonon spectrum $F(\Omega)$, containing the allowed phonon frequencies, varies per solid [8]. In real solids, these phonon spectra do not resemble analytical functions. According to Kaplan et al. [9], a useful approximation for the phonon spectrum of a material is the Debye approximation, where $\alpha^2(\Omega)F(\Omega) \approx b\Omega^2$, with b some constant (see figure 2.1) and $\alpha^2(\Omega)$ the effective electron-phonon coupling constant. This density of states is derived as follows: the Debye approximation uses a cutoff frequency ω_D to calculate the density of states and we have 3N vibrational modes in a crystal lattice. Thus

$$3N = \int d\vec{k} = 4\pi \int k^2 dk = \frac{4\pi}{v^3} \int \omega^2 d\omega = 9N \int_0^{\omega_D} \frac{\omega^2}{\omega_D^3} d\omega = \int_0^{\omega_D} g(\omega) d\omega, \tag{2.1}$$

with ω_D the Debye frequency. We can see that $g(\omega) \propto \omega^2$ [10]. Since the frequency of a phonon is directly related to its energy via $\Omega = \hbar\omega$, $\alpha^2(\Omega)F(\Omega) \approx b\Omega^2$ is a good approximation to use at low energies.

This description of lattice vibrations and the phonon spectrum will later be useful in describing processes in a superconducting solid.

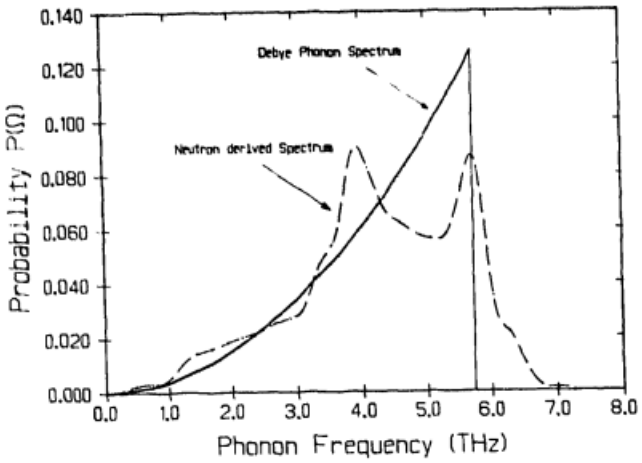

Figure 2.1: An experimentally measured phonon density of states of niobium (Nb, dashed line) along with its Debye approximation (black line). The Debye phonon spectrum stops abruptly at the Debye energy $\hbar\omega_D$ and note that the approximation is less accurate for higher phonon frequencies. Figure from Ref. [11].

2.2. Superconductivity

First discovered by H. Kamerlingh Onnes in 1911, superconductivity is a phenomenon where the resistivities of certain solids vanish below a certain critical temperature T_c (see figure 2.2). A very successful theory of superconductivity is BCS theory, named after its inventors: Bardeen, Cooper and Schrieffer. This theory predicts that below T_c an energy gap $\Delta(T)$ exists between normal electrons and electrons in a superconducting state. $\Delta(T)$ is temperature dependent, has a maximum $\Delta(0) = 1.76k_bT_c$ (at $T = 0$ K, with k_b the Boltzmann constant) and vanishes at $T = T_c$ (see figure 2.3). This energy gap allows two electrons to form a Cooper pair with a binding energy of 2Δ.

It seems counter intuitive that two electrons should be bound into pairs. One would expect to see the electrons repel each other because of the repulsive electromagnetic force between them, instead of the binding that is observed in Cooper pairs. However, this would only be the case for electrons that are completely free. Below T_c, electrons in a solid can exhibit an attractive interaction. When an electron moves through the crystal lattice, it slightly moves positively charged ions towards its position, leaving a higher positive charge density in its wake. This higher positive charge can attract another electron that drags behind the first electron (see figure 2.4). This pair of electrons is the Cooper pair described by BCS theory [12].

These Cooper pairs all share the same wave function to minimize their energies. This is possible because Cooper pairs consist of two electrons with opposing spins, totaling to zero combined spin. The Cooper pair thus behaves as a boson, which is allowed to share the same state with other bosons. Normally an electron behaves like a fermion, which can not occupy the same state as another fermion. In the bound state, the Cooper pairs no longer experience collision effects that cause resistivity in normal solids, resulting in the vanishing of the resistivity for a DC current seen in figure 2.2 [12].

Cooper pairs can be broken by photons or phonons with energies Q, $\Omega > 2\Delta$ respectively. When a Cooper pair is broken, two electrons, from here on referred to as quasiparticles, are “created” (see figure 2.5). The temporary change in the number of quasiparticles can be measured using an MKID. This will be explained in the next section.

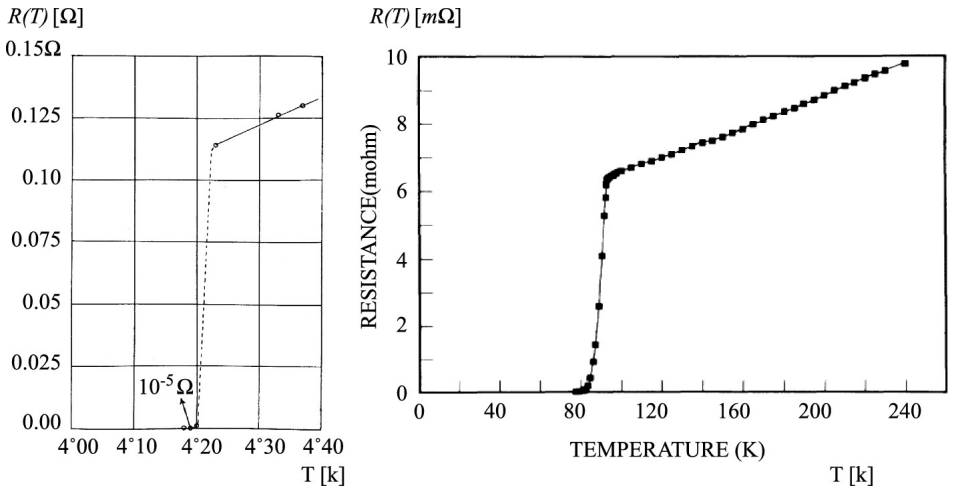

Figure 2.2: Vanishing resistance at critical temperature T_c of mercury (left, $T_c = 4.2$ K) and the high temperature superconductor $YBa_2Cu_2O_{7-x}$ (right, $T_c \approx 90$ K). Figure from Ref.[13]

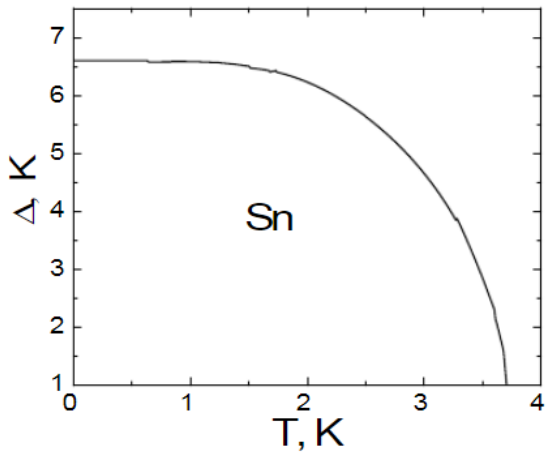

Figure 2.3: Temperature dependence of the superconducting gap value Δ in Sn. Note that the maximum value is at $\Delta(0)$ and the gap vanishes at T_c (3.7 K in this case). Note that Δ is given in units of temperature. Figure from Ref.[14].

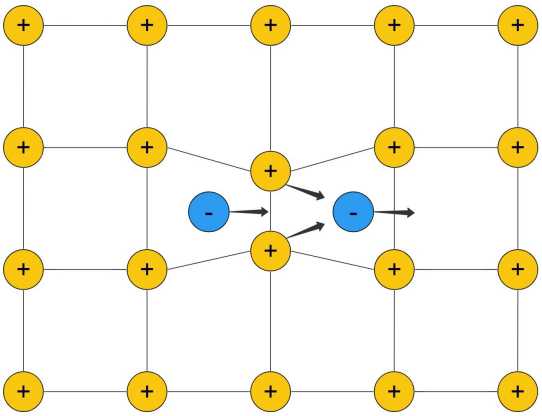

Figure 2.4: Schematic view of attractive interaction. When an electron moves through the crystal lattice, it slightly moves positively charged ions towards its position, leaving a higher positive charge density in its wake. This higher positive charge can attract another electron that drags behind the first electron.

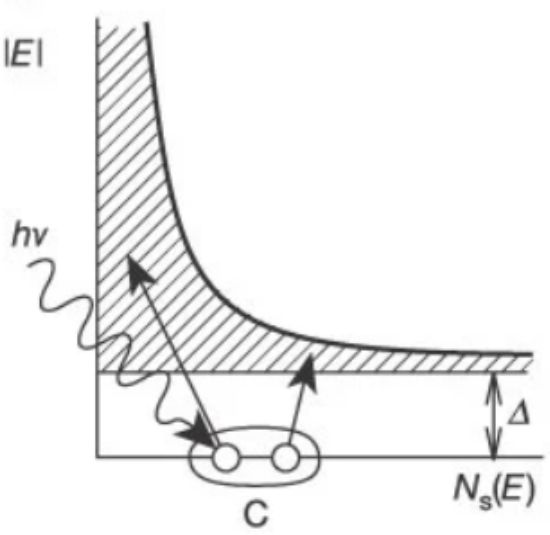

Figure 2.5: Photons with energy $hv > 2\Delta$ are absorbed by the superconductor, breaking Cooper pairs and creating a number of quasiparticles. In this figure, Cooper pairs (C) are shown at the Fermi level, and the density of states for quasiparticles, Ns(E), is plotted as the shaded area as a function of quasiparticle energy E. Figure and caption from Ref. [6].

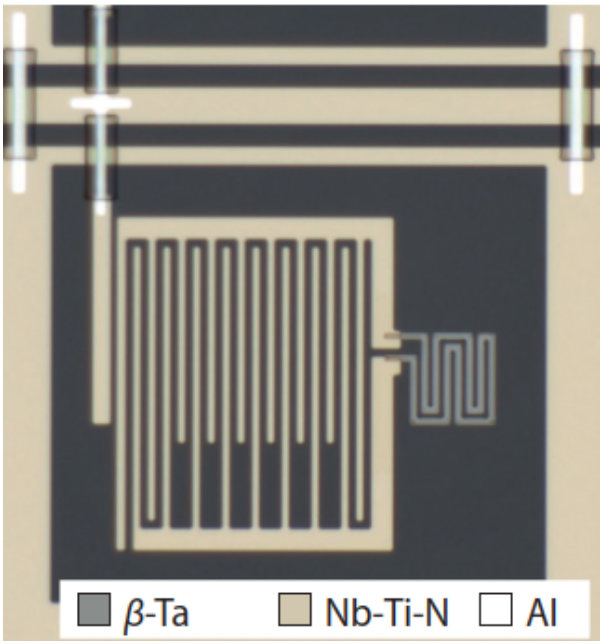

Figure 2.6: Microscope image of a Nb-Ti-N/β-Ta hybrid KID. One MKID has dimensions 150x150 μm. Here the Nb-Ti-N serves as a capacitor (center/left, goldish pattern) and β-Ta serves as the superconducting inductor (right, gray pattern). The inductor absorbs the photons that are measured by the MKID. The circuit is connected to a readout line at the top (see figure 2.7 for a schematic view). Figure from Ref. [5].

2.3. MKID detectors

2.3.1. Working principle

MKID detectors allow for the detection of single photons. Figure 2.6 shows a microscopic image of an MKID. Using a superconducting strip as an inductor, along with a capacitor, a resonant circuit with resonant frequency $f_0 = \frac{1}{LC_R}$ is created (see figure 2.7). Here $L = L_G + L_K$, with L_G and L_K the geometric and kinetic inductances respectively. An incoming photon can excite a number of quasiparticles in the superconductor, causing a change in L_K. This, in turn, causes as shift in the resonant frequency of the circuit. The system returns to its equilibrium state after a short time ($\approx$ 50 us [5]). Very small changes in the resonant frequency can be detected by measuring the phase shift θ of an AC readout signal. The magnitude of this phase shift can then be used to derive the wavelength of the incoming photon, because higher energy (shorter wavelength) photons cause a larger phase shift. Figure 2.8 shows the average phase shift of the readout signal of an MKID for different wavelengths of light as a function of time. For the scope of this report, the physical processes that allow for the detection of photons is most important. This will be elaborated in the following sections.

2.3.2. Response

In order to explain the response seen in figure 2.8, we investigate how changes in the number of quasiparticles N_{qp} in the superconductor impact the superconductors electrical properties. A photon absorbed by the superconductor causes excitations in the material in the form of quasiparticles and phonons. As mentioned before, phonons with energy $\Omega > 2\Delta$ can break Cooper pairs to create quasiparticles. Quasiparticles with $E > \Delta$ can emit phonons, which in turn can create more quasiparticles (given the emitted phonon's energy satisfies $\Omega > 2\Delta$). When the number of quasiparticles changes through this down-conversion process, the conductivity of the superconductor is affected. Gao et al [15] show that a change in the complex conductivity $\sigma = \sigma_1 - i\sigma_2$ of a superconductor is related to a

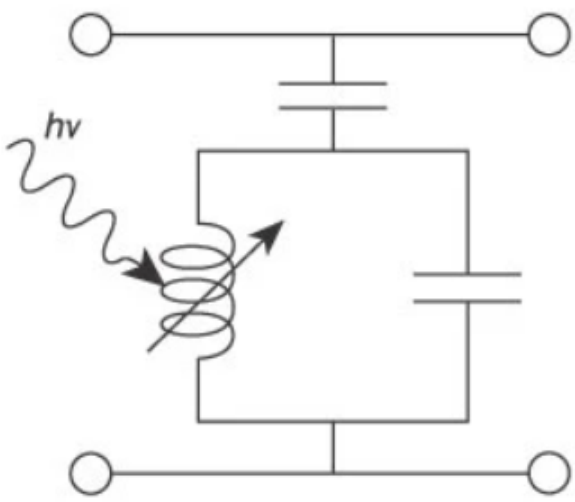

Figure 2.7: Schematic view of an MKID detector. A superconducting inductor $L = L_G + L_K$ and capacitor C_R act as a resonant circuit with resonant frequency $f_0 = \frac{1}{LC_R}$, which is monitored by a readout line. A photon with energy $h\nu > 2\Delta$ can excite quasiparticles in the superconducting inductor, changing its inductance and changing the resonant frequency of the circuit. This translates into the response seen in figure 2.8. Figure from Ref. [6].

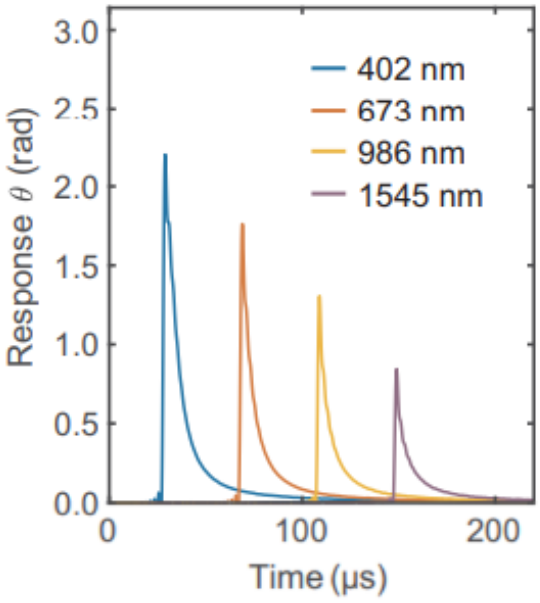

Figure 2.8: Average MKID detector response due to photon excitation for different wavelengths (average of about 1000 photons). The phase shift of the resonant frequency of the circuit is measured in order to detect individual photons and to calculate their energies. Figure from Ref. [5].

change in the quasiparticle density n_{qp} via

$$\frac{d\sigma_1}{dn_{qp}} = \sigma_n \frac{1}{N_0 \hbar\omega} \sqrt{\frac{2\Delta_0}{\pi k_B T}} sinh(\zeta) K_0(\zeta) \tag{2.2}$$

for the real part of the complex conductivity and

$$\frac{d\sigma_2}{dn_{qp}} = -\sigma_n \frac{\pi}{2N_0 \hbar\omega} \left[1 + \sqrt{\frac{2\Delta_0}{\pi k_B T}} e^{-\zeta} I_0(\zeta) \right] \tag{2.3}$$

for the imaginary part, with ω the angular frequency of the signal, $\zeta = \frac{\hbar\omega}{2k_B T}$, N_0 the density of states at the Fermi level for electrons of one spin orientation and does not include electron-phonon renormalization effects and I_0 and K_0 the modified Bessel functions of the first and second kind.

The change in the number of quasiparticles N_{qp} due to an incoming phonon can be observed through the amplitude A and phase of the readout signal of an MKID through [16]

$$\frac{dA}{dN_{qp}} = -\frac{\alpha_k \beta Q}{|\sigma| V} \frac{d\sigma_1}{dn_{qp}} \tag{2.4}$$

and

$$\frac{d\theta}{dN_{qp}} = -\frac{\alpha_k \beta Q}{|\sigma| V} \frac{d\sigma_2}{dn_{qp}}, \tag{2.5}$$

with α_k the fraction of kinetic inductance L_k over the total inductance L, $\beta = 1 + \frac{2d/\lambda}{sinh(2d/\lambda)}$ (with d the thickness of the superconducting film and λ the penetration depth of the magnetic field according to the London equation [12]), $Q = \frac{\omega E_{stored}}{P_{loss}}$ the quality factor of the resonant circuit (the amount of energy stored in the system divided by the energy loss per cycle), V the volume and $|\sigma| \approx \sigma_2$ for $T << T_c$. A change in the number of quasiparticles causes a shift in the resonant frequency, which causes the phase shift θ seen in figure 2.8.

2.3.3. Resolving power

The sensitivity of a single-photon counting MKID is in part given by its resolving power R. It is a dimensionless quantity that describes the MKIDs ability to distinguish two different wavelengths of light. In figure 2.9 one can see that different photons of the same wavelength can trigger varying responses from the MKID. If the response curves of two different wavelengths of light overlap because the wavelengths are close to each other, no distinction can be made between the two wavelengths. Higher resolving power means wavelengths closer to each other can be distinguished from each other. The most basic definition for resolving power is $R = \lambda/\Delta\lambda$, where $\Delta\lambda$ is the smallest wavelength difference that can be distinguished, shows how a high resolving power is beneficial for the functioning of an MKID. According to [5], the resolving power of an MKID is given by

$$R = \frac{1}{2\sqrt{2\ln 2}}\sqrt{\frac{\eta_{pb}Q}{\Delta(F+J)}}, \tag{2.6}$$

with Q the incoming energy and F the Fano factor (see section 2.5). There are a number of other variables in this equation that can limit the resolving power of an MKID. These will now be discussed.

Phonon loss

The phonon loss factor J represents the amount of hot phonons ($\omega > 2\Delta$) that are lost to the substrate around the superconducting film in the MKID. Research has suggested that it is possible to improve R by means of phonon trapping [17]. De Visser et al. [4] shows experimentally that the phonon loss factor can now be improved to $J = 0.11$. This is assuming $F = 0.2$, since F and J cannot be measured separately, but need to be derived from resolving power measurements. Figure 2.10 shows that the measured resolving power of an MKID is restricted more by the contribution of the Fano factor than the contribution of the phonon loss factor. Thus the term $(F + J)$ in the resolving power is restricted mainly by the Fano factor. In the simulation that will be performed, we take $J = 0$, because we will be modeling for Fano-limited MKIDs.

Pair breaking efficiency

The pair breaking efficiency η_{pb} is the amount of energy of the incoming photon that is efficiently used to break Cooper pairs. So for each Cooper pair that is broken, 2Δ energy is used effectively. $\eta_{pb} = 1$ means that all photon energy is used to make quasiparticles with energy level Δ, so that $N_{qp} = Q/\Delta$. Previous studies have shown that $\eta_{pb} \approx 0.60$ [11][18]. This again means that 60% of the photon energy is used to create quasiparticles at energy Δ.

Gap energy

The gap energy Δ, as mentioned before, is the amount of energy needed to create one quasiparticle, so that 2Δ is needed to break one Cooper pair. Materials with a lower gap energy allow more quasiparticles to be created from the same photon energy Q. However, since $\Delta(0) = 1.76k_bT_c$, we need a lower working temperature for an MKID if we choose a detector material with a lower gap energy. Since current detectors already operate in the range of 100 mK, lowering the working temperature even further is impractical and efforts should be made to improve other MKID properties, like the Fano factor, first.

Signal to noise power

Another quality property in MKIDs is the signal to noise ratio, or the noise equivalent power (NEP). This quality tells us how much power a signal must have to be distinguishable from noise in the detector. According to De Visser [16], the noise equivalent power is defined as the power which can be detected with a signal-to-noise ratio of one with a bandwidth of 1 Hz. A lower NEP means a more sensitive detector. Figure 2.10 shows that the signal to noise contribution to the resolving power (R - Signal-to-noise in the figure) is not the limiting factor in the resolving power of an MKID. We can clearly see that the Fano-limited contribution of the resolving power (black line) has the biggest contribution towards limiting the resolving power of an MKID.

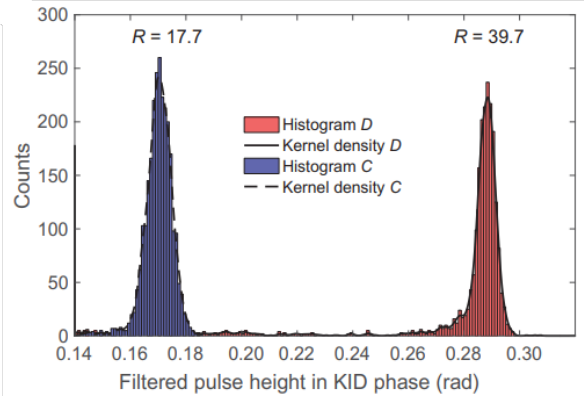

Figure 2.9: Histogram of pulses of two MKIDs C and D at 120 mK, illuminated with the 673-nm laser and with P = -83 dBm and P = -85 dBm, respectively. The spread seen in the filtered pulse height illustrates the resolving power of the MKID. Figure from Ref.[17]

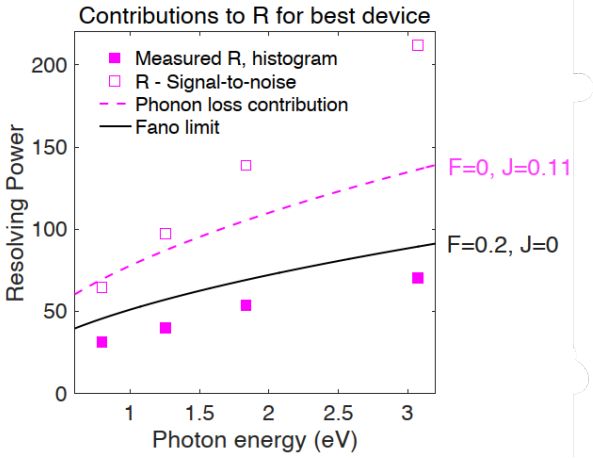

Figure 2.10: Different contributions to the resolving power of an MKID as a function of the photon energy with different values of F and J. The contributions add following $\frac{1}{R^2} = \frac{1}{R_1^2} + \frac{1}{R_2^2}$.... Note that the measured resolving power is closest to the line where only the Fano factor limits the resolving power of the MKID, and thus the chip is limited mostly by F. Figure from Ref. [4].

2.4. Interactions

To eventually model the behaviour of the superconductor, we need to understand the mechanism behind the creation of excess quasiparticles. The down-conversion process from a photon to a number of quasiparticles is illustrated by figure 2.11. A photon with energy $Q > 2\Delta$ interacts with the detector, breaking a single Cooper pair and transferring most of its energy to one quasiparticle (E_0). This high energy particle quickly shares its energy with a number of quasiparticles. The quasiparticles that are created (E_1) then send out phonons that, in turn, can break more Cooper pairs [9][19]. This reaction continues until no more Cooper pairs can be broken. The resulting net change in the number of quasiparticles N_{qp} influences the kinetic inductance of the superconducting material, which can be measured as described in section 2.3.2. The excess quasiparticles eventually recombine into Cooper pairs while emitting phonons [9], and the response curve in figure 2.8 returns to its equilibrium state.

Kaplan et al. [9] shows that the rate of Cooper pair breaking by a phonon of energy Ω is given by

$$\tau_B^{-1}(\Omega) = \frac{4\pi N_0 \alpha^2(\Omega)}{\hbar I} \int_\Delta^{\Omega-\Delta} \frac{dE}{(E^2-\Delta^2)^{1/2}} \times \frac{E(\Omega-E)+\Delta^2}{[(\Omega-E)^2-\Delta^2]^{1/2}}, \tag{2.7}$$

where I denotes the ion number density.

The phonon emission rate by a quasiparticle with energy E is given by

$$\tau_s^{-1}(E) = \frac{2\pi}{\hbar Z_1(0)} \int_0^{E-\Delta} d\Omega \alpha^2(\Omega) F(\Omega) \times \frac{E-\Omega}{[(\Omega-E)^2-\Delta^2]^{1/2}} \times \left(1 - \frac{\Delta^2}{E(E-\Omega)}\right), \tag{2.8}$$

where $Z_1(E)$ is the real part of the renormalization parameter which appears in determining the poles of the single-particle Green's function in the superconducting state and is assumed to be energy independent by setting E = 0. [18]

In section 3.3, equations 2.7 and 2.8 are used to derive the probability distributions for pair breaking and phonon emission.

Other interactions that occur are phonon absorption by a quasiparticle, recombination of quasiparticles with phonon emission and phonon/electron scattering. However, these processes are either irrelevant for the calculations that will be done, or have lifetimes that are very large compared to equations 2.7 and 2.8, where a long lifetime means the interaction is unlikely to happen compared to an interaction with a short lifetime. These interactions can be neglected. This will be shown in section 3.2.

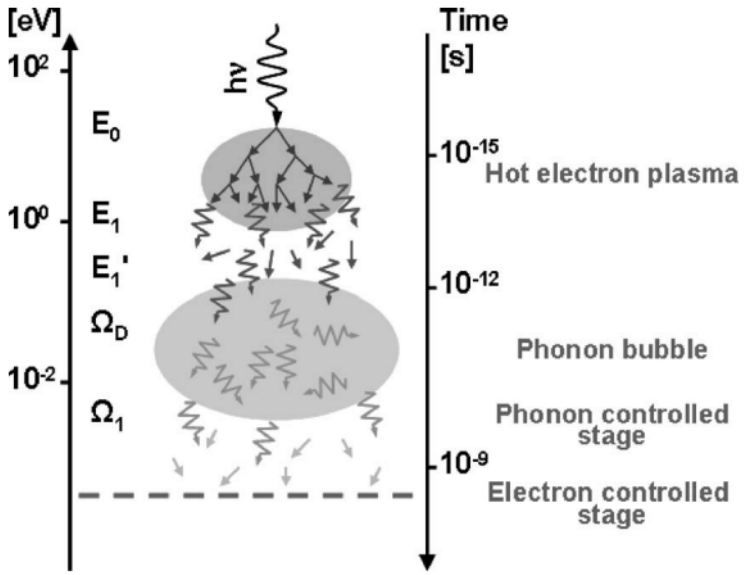

Figure 2.11: Schematic view of the downconversion process. A photon with energy $Q > 2\Delta$ interacts with the detector, breaking a single Cooper pair and transferring most of its energy to one quasiparticle (E_0). This high energy particle quickly shares its energy with a number of quasiparticles. The quasiparticles that are created (E_1) then send out phonons that, in turn, can break more Cooper pairs [9][19]. Figure from Ref. [19].

2.5. The Fano Factor

Interactions on molecular level are subject to uncertainties in outcomes of processes due to the statistical properties of the physics governing these systems. A measure for such uncertainties is the Fano factor. First defined by Ugo Fano [20] to measure noise in ion detectors, the Fano factor is given by

$$F = \frac{\langle (n - \langle n \rangle)^2 \rangle}{\langle n \rangle}, \tag{2.9}$$

where n is the number of events and $\langle n \rangle$ the average number of events. As seen in equation 2.6, the Fano factor F plays a role in the maximum resolving power that can be achieved in an MKID detector. The Fano factor in this case represents the statistical uncertainty in the downconversion of an incoming photon into a number of quasiparticles. Now equation 2.9 can be written in terms of the number of excess particles N_{qp}:

$$F = \frac{\sigma^2_{N_{qp}}}{\langle N_{qp} \rangle}, \tag{2.10}$$

where $\sigma^2_{N_{qp}} = \langle (N_{qp} - \langle N_{qp} \rangle)^2 \rangle$ is the standard deviation in the number of excess quasiparticles N_{qp} in the material. Previous research has found values of $F = 0.195 \pm 0.01$ for Sn and $F = 0.22 \pm 0.01$ for Nb [18][11]. $F \approx 0.2$ is often used in calculations of resolving power for MKIDs [5][17][21]. As mentioned before, the central question in this report is whether and how this Fano factor may be improved.

From equation 2.10 is apparent how the Fano factor might, in theory, improve. Either by decreasing $\sigma_{N_{qp}}$ and/or increasing $\langle N_{qp} \rangle$ the Fano factor becomes smaller, improving the resolving power in equation 2.6. As mentioned in section 2.3.3, the resolving power of an MKID is now limited by F. Finding a way to improve F could result in an improvement in the resolving power of MKIDs.

3

Simulation

This chapter will describe how the simulation used to calculate the Fano factor was constructed. The calculation methods (3.1 and 3.3) and assumptions about the simulation (3.2) are discussed and the simulation is validated (3.7). The simulation was written in python. The files containing the code have been made available on Github[1].

3.1. Simulation method

In order to accurately calculate the Fano factor from equation 2.10, we must collect a lot of datapoints for N_{qp}. In order to collect this data, a Monte Carlo simulation simulating a photon interacting with a superconductor was created. The equations from Kaplan et al. [9] are used to describe the phonon-quasiparticle interactions, which is elaborated is sections 3.2 and 3.3.

Because we are simulating a large number of particles (in the order of 10^3), an appropriate method of calculation is required to minimize computation times. While most of the script is fairly straightforward, the method for deciding the outcomes of interactions (i.e. what energies created quasiparticles have after a phonon breaks a Cooper pair) was a challenge. A brute force method, where from the density of states the cumulative distribution function was repeatedly calculated for each particle that interacted, proved too slow for a Monte Carlo simulation (minutes per simulated photon). This was due to the integration function that was called thousands of times per cycle. Another method that was tried was by means of a rejection envelope, where samples are randomly drawn and discarded or kept based on some threshold [22]. This method proved inaccurate and thus was unsatisfactory as well. Finally a similar method to Kurakado [18] was used. With this method, a group of phonons with energy equal to the photon energy is initialised at the start of each simulation. This method gives an upper and lower bound for the phonon ($0 < \Omega < \hbar\omega_{max}$) and quasiparticle ($\Delta < E < \hbar\omega_{max} - \Delta$) energies, the latter since two quasiparticles which both need to have a minimum of $E = \Delta$ energy are created by a phonon, giving $E = \hbar\omega_{max} - \Delta$ for the maximum quasiparticle energy. In reality, quasiparticles may have energies above the Debye energy [19].

The energy bounds are discretized into energy bins with bin width equal to a chosen stepsize, with the bin energy given by the energy at the middle of the bin (see the green and black lines in figure 3.3). This method also allows for both phonon en quasiparticle energies to be defined along one energy array that ranges from half a stepsize to the Debye energy in steps equal to the stepsize.

This definition of the energy raises an issue however, because when a pair breaking or emission interaction takes place, the energy of the interaction is not conserved. For example (at a stepsize of $1/10\Delta$, a phonon with energy 2.05Δ can create two quasiparticles at energy 1.05Δ. The total quasiparticle energy appears to be $1.05\Delta + 1.05\Delta = 2.1\Delta$ and thus energy would not be conserved. This apparent issue can be resolved when we realize that the ”real” energy of a particle can fall anywhere within its bin. A quasiparticle assigned to the 1.05Δ bin can have energies from $1\Delta \leq E \leq 1.1\Delta$. So

[1] `https://github.com/Aaron3335/BEP_Fano_factor.git`

a 2.05Δ phonon (which can have $2\Delta \leq \Omega \leq 2.1\Delta$) can always make two quasiparticles that fall into the $1\Delta \leq E \leq 1.1\Delta$ quasiparticle bin. This solves our conservation issue. The end of this chapter will show that the unconserved energy is only about 0.02% of the total energy at the stepsize we choose.

Prior to running the simulation, all probabilities and outcomes for all possible quasiparticle and phonon interactions are calculated, and these probabilites are used during the simulation to randomly decide the outcomes of interactions. This discretization process is further elaborated in section 3.3.

These discretization calculations typically take a couple seconds, depending on stepsize chosen for the energy bins (see figure 3.14). All calculations were performed in units of Δ for simplicity.

3.2. Assumptions

To model the quasiparticle-phonon-photon interactions in the superconductorns, a number of assumptions must be made. Firstly, we assume Δ to be independent of temperature. For low fractions T/T_c this is a fair assumption (see figure 2.3) and since MKIDs typically operate at $T/T_c \approx 0.1$ we can use this approximation. We use the value of Δ at $T = 0$ K.

Secondly, we assume that there is no phonon loss to the environment and thus all phonons interact within the superconducting material. In reality this loss is accounted for by the phonon loss factor J in equation 2.6, but since we are modeling for the Fano limit we assume $J = 0$.

Thirdly, we assume Cooper pair breaking by a phonon and phonon emission by a quasiparticle are the only interactions that take place within our system. We do not take in account the following processes:

Quasiparticle recombination

In a real solid, quasiparticles that are created eventually recombine into Cooper pairs while emitting a phonon. Figure 3.1 shows that, at the working temperature of an MKID ($0.1T/T_c$), the quasiparticle recombination lifetimes τ_r are very long compared to the lifetime of phonon emission by a quasiparticle τ_s. This means the rate of quasiparticle recombination is very small compared to the rate of phonon emission, which means the first process is way less likely to take place compared to the latter.

Phonon scattering

Another process that takes place in a real material is phonon scattering. Figure 3.2 shows that, for the working temperature of an MKID, the phonon scattering rates τ_{phs}^{-1} are very small compared to the rate τ_B^{-1} at which phonons break Cooper pairs. Note that the scattering rate is the inverse of the scattering lifetime and a low rate means the same as a long lifetime. We can ignore the phonon scattering process on the same basis as the quasiparticle recombination process.

Phonon absorption

The last process we ignore is the absorption of a phonon by a quasiparticle. Absorption of a phonon by a quasiparticle is neglected because this quasiparticle would then eventually emit this phonon again through equation 2.8, essentially undoing the interaction. This process would have no effect on the outcome of the simulation.

Lastly we use the Debye approximation $\alpha^2(\Omega)F(\Omega) \approx b\Omega^2$. Values for $\alpha^2(\Omega)F(\Omega)$ are typically fitted to this function for energies below 1.6 meV ($\approx 6\Delta$ for Sn) [23]. Because the outcome of the simulation only depends on the spectrum at low energies (all high energy phonons and quasiparticles eventually scatter into low energy states $0 < E < 3\Delta$, which is in this low energy limit), we use the approximation instead of experimental data. Earlier research has shown that this assumption has negligible effect on the outcome of the simulation [11] and section 3.7 will show this also holds for this simulation.

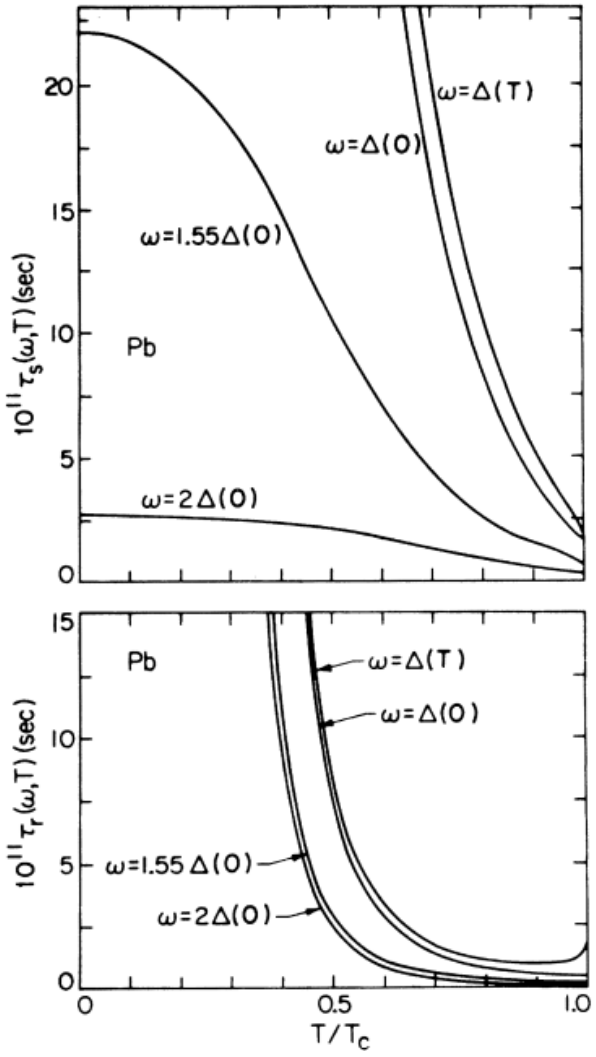

Figure 3.1: Lifetime of photon emission by a quasiparticle τ_s and the quasiparticle recombination time τ_r as a function of T/Tc for Pb. Note that for our regime ($T/T_c < 0.5$), the recombination time for quasiparticles with $E > 2\Delta$ is very long compared to the emission time. Thus we neglect recombination effects. Lifetimes of quasiparticles with $E < 2\Delta$ do not fall in this negligible regime. However, these quasiparticles cannot emit pair breaking phonons ($\Omega > 2\Delta$). Since we are only interested in the behaviour of quasiparticles with $E > 3\Delta$ that can emit pair breaking phonons, we can still neglect the recombination effects. Figure from Ref. [9].

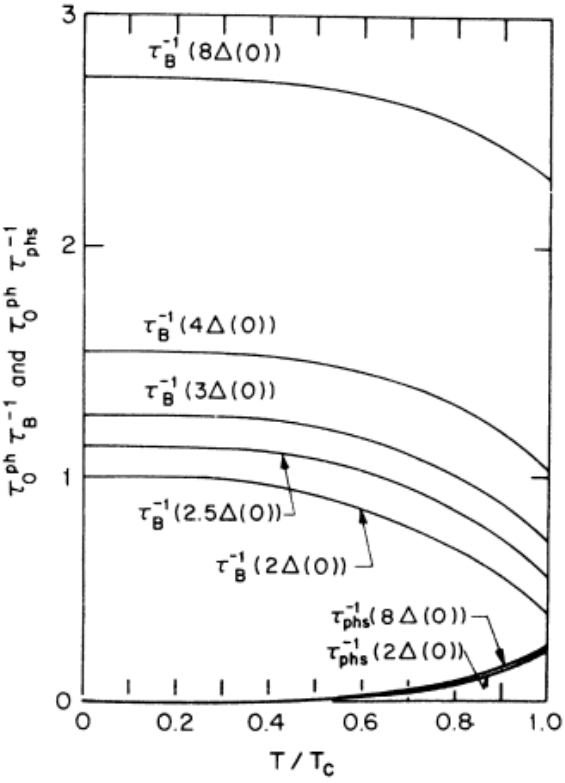

Figure 3.2: The Cooper pair breaking rate by a phonon τ_b^{-1} and the phonon scattering rate τ_{phs}^{-1} as a function of T/T_c. Note that in our regime ($T/T_c < 0.5$) the rate of phonon scattering is very small compared to the Cooper pair breaking rate. Thus we neglect phonon scattering effects. Figure from Ref. [9].

3.3. Distributions

We need to describe the probabilities of all interactions relevant to the production of excess quasiparticles. In this section three distributions will be derived. One for the initial phonon group used to start the simulation, one for the pair breaking interaction and one for the phonon interaction.

For our simulation we do not model the first part of the down-conversion process. Instead we initialize a group of phonons which total energy equals the photon energy Q. The distribution is based on the Debye approximation $\alpha^2(\Omega)F(\Omega) \approx b\Omega^2$. The probability distribution of the initial phonon group is then given by:

$$P_\Omega(\Omega) = \alpha^2(\Omega)F(\Omega) \times \frac{1}{A} \approx b\Omega^2 \times \frac{1}{A}, \tag{3.1}$$

with $P_\Omega(\Omega)$ the chance of a phonon with energy Ω being created in the initial phonon group where the values of Ω are based on the chosen step size. A is the normalisation factor with $A = \sum_{\Omega=0}^{\Omega_{max}} P_\Omega(\Omega)$. A for the real phonon spectrum probability distribution can also be obtained by taking experimental data of phonon spectra, fitting the approximation to the data at low energies and normalising it in a similar fashion as described above.
The second and third distributions are obtained by taking the integrands from equations 2.7 and 2.8, resulting in the probability densities for the pair breaking interaction $\Omega \to E + E'_{\Omega-E}$ and the phonon emission interaction $E \to E'_{E-\Omega} + \Omega$.

The second distribution gives the chance a phonon with energy Ω creates a quasiparticle with energy E.

$$P_{\Omega\to E}(\Omega, E) = \frac{1}{(E^2-\Delta^2)^{1/2}} \times \frac{E(\Omega-E)+\Delta^2}{[(\Omega-E)^2-\Delta^2]^{1/2}} \times \frac{1}{B}, \tag{3.2}$$

Where $P_{\Omega\to E}(\Omega)$ is the probability of a phonon with energy Ω producing a quasiparticle with energy E. Note that a phonon always produces two quasiparticles, one with energy E as described above and one with energy $E' = \Omega - E$, as energy is conserved. Normalisation factor B is given by $B = \sum_{E=\Delta}^{\Omega-\Delta} P_{\Omega\to E}(\Omega, E)$.

The third distribution gives the chance that a quasiparticle with energy E emits a phonon with energy Ω:

$$P_{E\to\Omega}(E, \Omega) = \alpha^2(\Omega)F(\Omega) \times \frac{E-\Omega}{[(\Omega-E)^2-\Delta^2]^{1/2}} \times \left(1 - \frac{\Delta^2}{E(E-\Omega)}\right) \times \frac{1}{C}, \tag{3.3}$$

with $P_{E\to\Omega}(\Omega)$ probability of a quasiparticle with energy E emitting a phonon with energy Ω.
$C = \sum_{\Omega=0}^{E-\Delta} P_{E\to\Omega}(E, \Omega)$, similar to B.

This method causes an issue when calculating the last bin probabilies of equation 3.2,
where $\lim_{\Omega\to E-\Delta} \frac{1}{((\Omega-E)^2-\Delta^2)^{1/2}} = \infty$ and in equation 3.3, where $\lim_{E\to\Omega-\Delta} \frac{1}{((\Omega-E)^2-\Delta^2)^{1/2}} = \infty$. This occurs because the last bin energy is exactly on the infinite probablity density at $E = \Omega - \Delta$. To prevent throwing away this bin, which does contain valid states, we simply take the energy of the last bin to be at a quarter step size from the bin edge instead of half a step size (see figure 3.3). This also means we need to account for the fact that this bin is half as wide compared to the other bins. This can be accounted for by dividing the last bins probability by two.

The resulting distributions, along with samples drawn from these distributions are shown in figures 3.4 to 3.7. A large number of these distrutions will be calculated for all allowed energies Ω and E. The results of these calculations provide all the information needed to perform the simulation.

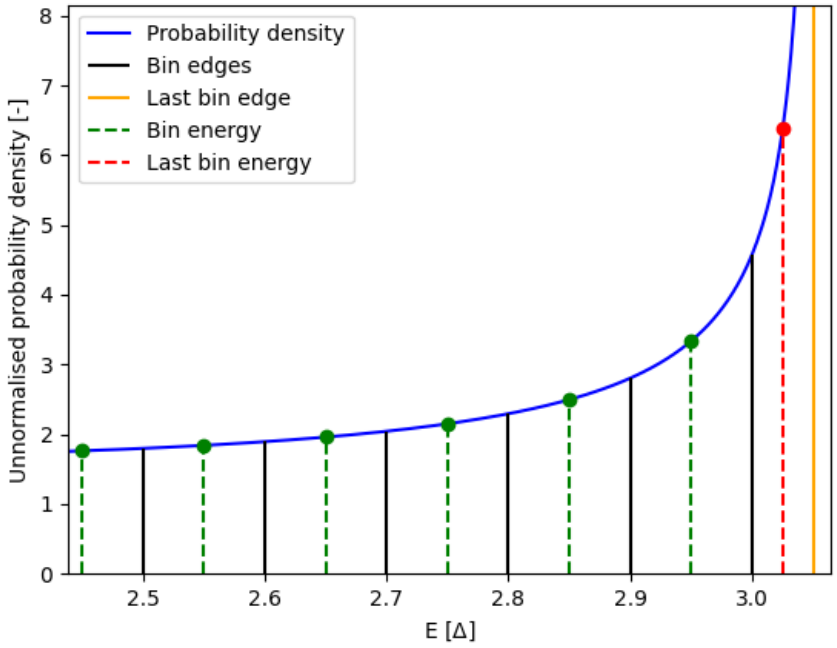

Figure 3.3: Right hand side of the pair breaking probability distribution for a phonon with bin energy $\Omega = 4.05\Delta$ (stepsize = $\Delta/10$). The y-axis indicates the chance that a phonon with energy $\Omega = 4.05\Delta$ creates a quasiparticle at energy E. Quasiparticles are always created in pairs, so this process also creates another quasiparticle at $E' = \Omega - E$. The full distribution is shown in figure 3.6. The figure shows that the last bins energy is moved a quarter stepsize to the left. The right edge is moved half a stepsize to the left. This causes the width of the last bin to be half the normal stepsize. This is accounted for in the calculation of probabilities by dividing the last probability by 2.

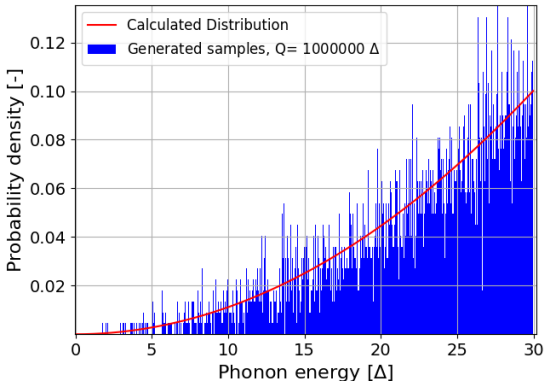

Figure 3.4: The phonon distribution given by the Debye approximation in equation 3.1 (red), along with random samples drawn from the distribution (blue). Note that because the distribution is normalised, the value of b in equation 3.1 does not matter.

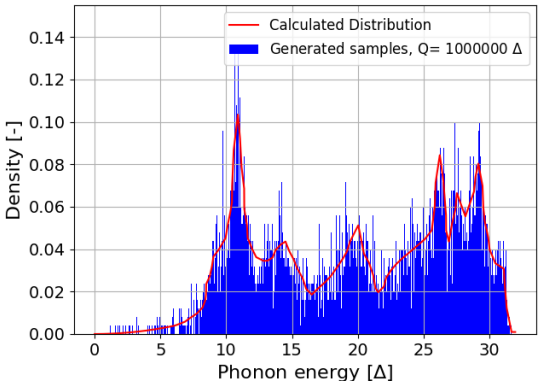

Figure 3.5: The phonon distribution of tin (Sn, red), along with random samples drawn from the distribution (blue).

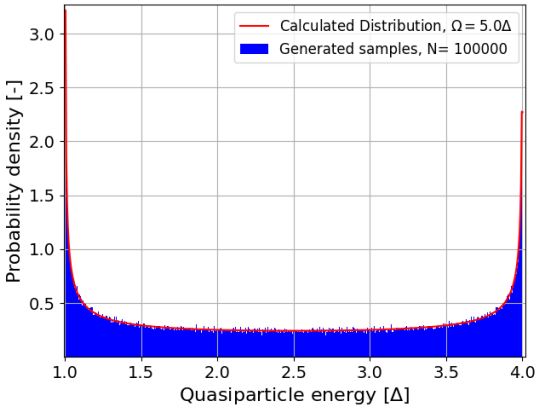

Figure 3.6: The pair breaking distribution for a phonon with $\Omega = 5\Delta$ (red), along with random samples drawn from the distribution (blue). Note that the distribution of the samples is perfectly symmetrical, because for each created quasiparticle with energy E, another with energy $E' = \Omega - E$ is created. The right hand side of the distribution is lower than the left, because of the division by 2 of the last bin to account for its reduced width (see figure 3.3).

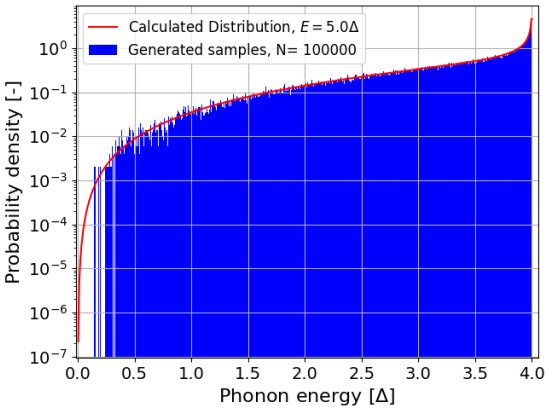

Figure 3.7: The phonon emission distribution for a quasiparticle with energy $E = 5\Delta$ (red), along with random samples drawn from the distribution (blue). Note that this distribution was calculated with the Debye approximation for the phonon spectrum: $\alpha^2(\Omega)F(\Omega) \approx b\Omega^2$. Using experimentally determined phonon spectra like in figure 2.1 produces different results for this distribution.

3.4. Simulation parameters

There are three parameters that are important for the simulation. The first is the energy of the incoming photon Q, which determines the amount of initial phonons created via equation 3.1 (see figure 3.4), or an experimentally determined phonon distribution as seen in figure 3.5. Larger Q negatively influences the computation time needed for the simulation, since more quasiparticles will be created, which takes longer to compute. Another free variable is the choice of superconducting material, which determines the phonon spectrum (when not using the Debye approximation) and determines the maximum phonon energy via the Debye temperature $\hbar\omega_D$. The Debye temperature also determines the maximum quasiparticle energy in this case, as we start our simulation with a initial phonon group with $\Omega_{max} = \hbar\omega_D$, and thus $E_{max} = \Omega_{max} - \Delta$ (keep in mind that in reality, quasiparticles may have higher energies). The choice of material also determines the magnitude of Δ. Table 3.1 gives some material properties of different metals. The last parameter that we can modify are band gaps in the phonon spectrum. This will be elaborated in section 4.1.5.

Table 3.1: The gap energy at 0 K, Debye temperature and critical temperature of the metals used in this report. Data from Ref. [24] and Ref. [25].

Material	$\Delta(0)$ [meV]	ω_D [K]	T_c [K]
Al	0.17	433	1.2
Sn	0.575	200	3.7
Nb	1.525	276	9.3

3.5. Procedure

Figure 3.8 shows how different parts of the simulation fit together. Firstly, all the outcomes and probabilities corresponding to the pair breaking and phonon emission interactions are calculated. Then a group of initial phonons is created according to equation 3.1, with their combined energies equal to the photon energy Q.

After this initialisation, phonons with $\Omega > 2\Delta$ break Cooper pairs according to equation 3.2, creating quasiparticles. Quasiparticles with energy $E > 3\Delta$ then emit a phonon according to equation 3.3. These pair breaking and emission steps are repeated until there are no more pair breaking phonons

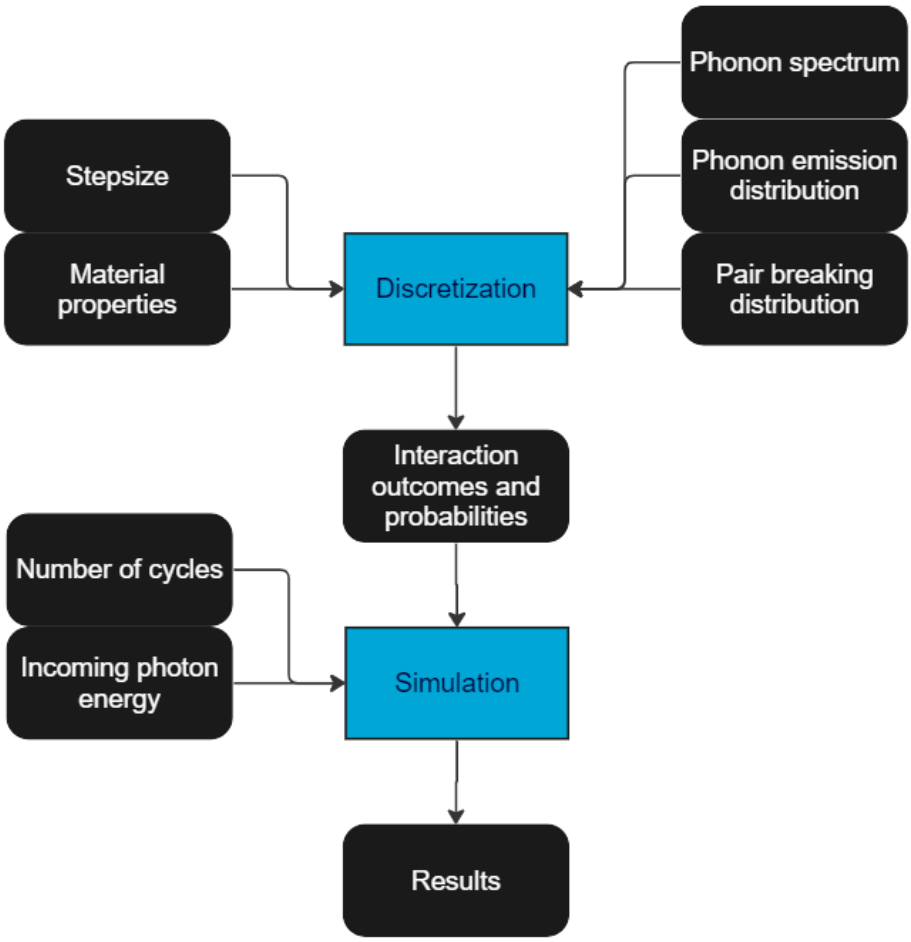

Figure 3.8: Overview of the different parts of the simulation. Based on the simulation parameters and distributions the discretization is calculated, after which the simulation is performed. Here the interactions and outcomes are used to calculate how many quasiparticles are generated, along with what energies the quasiparticles and phonons that are generated have. The simulation process is repeated the desired amount of times to simulate a large number of photons. The results are then saved for analysis.

($\Omega_{max} < 2\Delta$) and there are no quasiparticles left that can emit pair breaking electrons ($E_{max} < 3\Delta$). This process is repeated a set amount of times to form a dataset with excess quasiparticles N_{qp}, from which F can be calculated. The results will be shown in the next chapter.

3.6. Time evolution

To study the quasiparticle and phonon populations as a function of time, a separate simulation was set up that calculates the time it takes for pair breaking and phonon emission to take place based on the lifetimes of each phonon and quasiparicle energy according to equations 2.7 and 2.8. This version of the simulation calculates the interactions of the quasiparticles and phonons through discrete time steps. The constants used for the calculations are listed in table 3.2. Note that we use the mean value for $\alpha^2(\Omega)$. The results are shown in the section 4.1.1.

Table 3.2: Values for the variables that appear in equations 2.7 and 2.8, for the metals used in this report. Data from Ref. [9].

	N_0 [10^{21} states/eV]	I [10^{22} ions/cm^3]	$\langle\alpha^2(\Omega)\rangle$ [meV]	$Z_1(0)$ [-]	b [10^3 meV$^-2$]
Al	12.2	6.02	1.93	1.43	0.317
Sn	8.14	3.70	1.14	1.72	2.32
Nb	31.7	5.57	4.6	2.84	4.0

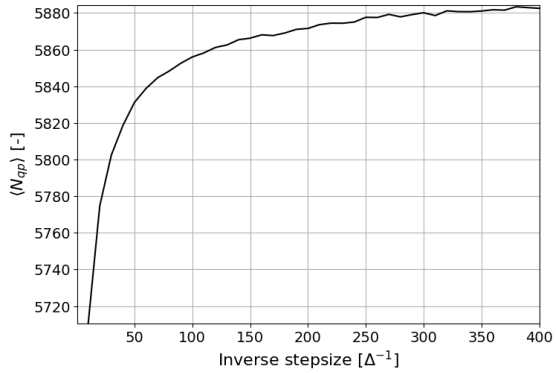

Figure 3.9: Mean values of N_{qp} for 3000 simulated photons as a function of the inverted stepsize. Note that N_{qp} converges.

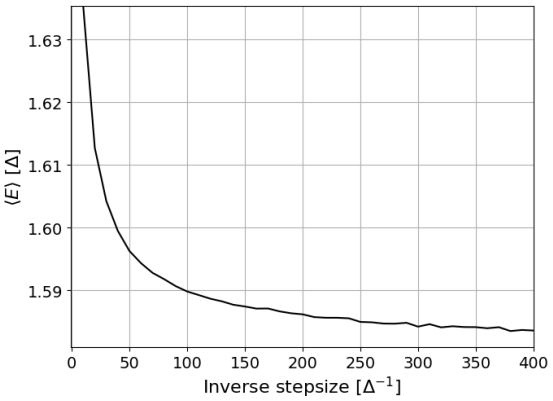

Figure 3.10: Mean values of E for 3000 simulated photons as a function of the inverted stepsize. Note that E converges.

3.7. Validation of the simulation method

To check whether or not our simulation provides useful results, some validation checks were performed. These checks use the same parameters as Kurakado [18] (material parameters for tin, $Q = 10^4\Delta$). Figure 3.9 shows the mean number of generated quasiparticles $\langle N_{qp} \rangle$ as a function of the inverted stepsize. Figure 3.10 shows the same for the mean quasiparticle energy $\langle E \rangle$. Both $\langle N_{qp} \rangle$ and $\langle E \rangle$ converge for smaller stepsizes. This is a sign that our simulation is valid. Figure 3.11 shows that the value of the Fano factor has has no significant dependency on the chosen step size.

The usage of the Debye approximation or the real phonon spectrum (with the Debye approximation fitted to the spectrum for low energies) proved to have little effect on the outcome of the simulation (≈ 0.2% with a stepsize of $1/200\Delta$). Therefore we will use the Debye approximation for the rest of our simulations. This indifference is in agreement with earlier research [11].

Figures 3.13 and 3.14 the computation time of a single photon and the time it takes for the discretization process to complete as a function of the inverted stepsize. Smaller stepsizes logically mean longer computation times. For the rest of this report, we will use a stepsize of $1/200\Delta$, to balance accuracy with simulation speed. This allows for many data points to be collected without losing much accuracy and without taking too much time. The energy deficiency due to the issue that a phonon can create two quasiparticles which have a combined energy that is higher than the phonon energy (see section 3.1) is plotted in figure 3.12 and is sufficiently low ($\approx 0.02\%$) to be neglected.

The value of $\langle N_{qp} \rangle$ seem to converge to $\langle N_{qp} \rangle \approx 5900$ as the stepsize approaches zero, which is a 0.5% difference compared to the result of Kurakado [18]. While efforts were made to completely reproduce the results of Kurakado and Rando et al. [11], their descriptions of their simulations in their respective articles are rather short, and thus it is difficult to pinpoint the cause of the discrepancy between the results. We consider the difference acceptable given the likely different numerical implementations and continue with this model.

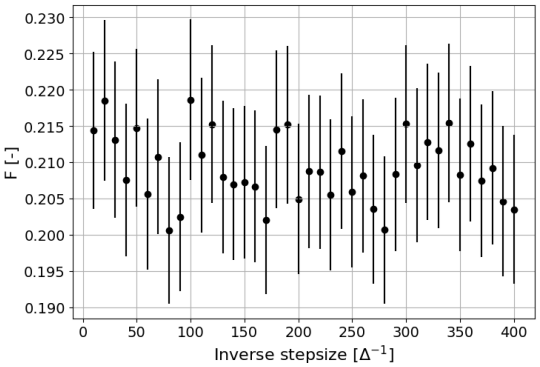

Figure 3.11: The value of F for 3000 simulated photons as a function of the inverted step size. The uncertainties in F are derived in section 4.1.2. A smaller stepsize has no significant effect on the value of F. Note that we will perform more simulate more photons for each data point chapter 4, resulting in smaller uncertainties on F.

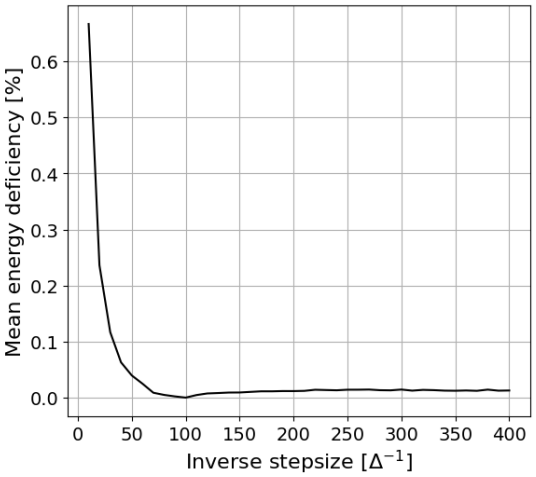

Figure 3.12: The mean difference between the starting energy ($10^4\Delta$ in this case) and the energy stored in phonons and quasiparticles at the end of a simulation as a function of the inverse stepsize. This energy deficiency is due to the fact that in this simulation, a phonon can create two quasiparticles with a combined energy higher than the phonon energy, as described in section 3.1.

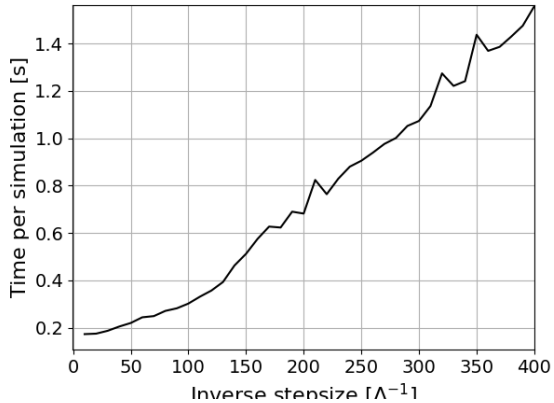

Figure 3.13: The time it takes for the simulation of one photon hitting superconducting Sn as a function of the inverted step size. Multiplication of the y-axis with the number of simulated photons gives the approximate simulation time (i.e. 3000 photon simulations and a stepsize of 1/200 would take approximately 35 minutes). Note that the stepsizes on the x-axis are inverted, so the right side represents a smaller stepsize.

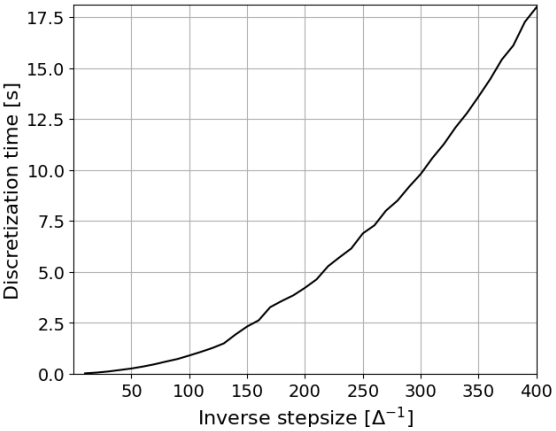

Figure 3.14: The time it takes to discretize the outcomes and probabilities of the interactions that take place in the simulation as a function of the inverted stepsize. The material properties used are those of tin. Smaller stepsizes take significantly longer to discretize.

4

Results and discussion

This section presents the results of varying experiments performed with the simulation, including testing different material inputs, different photon energies and different phonon spectra. The errors on the results are derived. The simulation results, possible improvements for the simulation and real world applications are discussed.

4.1. Results

4.1.1. Time evolution

Figure 4.1 shows the population of the number of quasiparticles N_{qp} and the number of phonons N_{Ω} in superconducting niobium as a function of time. We can see that the number of pair-breaking phonons ($\Omega \geq 2\Delta$) quickly reaches a maximum and then completely depletes within 2 ns. The number of quasiparticles reaches its maximum in the same time interval. This figure provides a useful insight in how the down-conversion process from a photon to a number of quasiparticles behaves. Keep in mind that for the rest of the results the calculations were performed without taking in account time steps, but by assuming that every quasiparticle and phonon that can interact eventually interacts. This has no impact on the results.

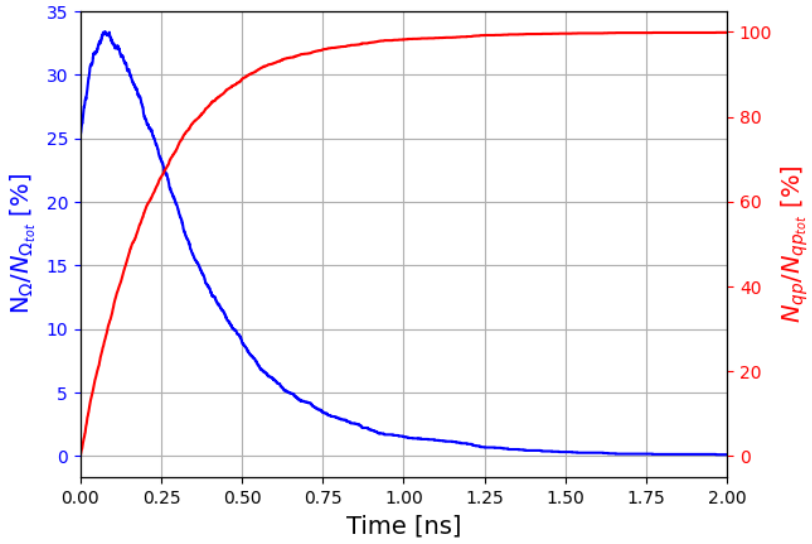

Figure 4.1: The excess quasiparticle and phonon populations after photon absorption in superconducting niobium as a function of time. The populations are shown as the percentage of the total amount of generated quasiparticles or phonons in the entire process.

4.1.2. Errors

Before the rest of the results are shown, the derivation of the errors in the experimental results will be presented. The calculation of the uncertainty in the experimentally determined Fano factors are not trivial. Because the Fano factor is defined as $F = \frac{\sigma^2_{N_{qp}}}{\langle N_{qp} \rangle}$, we need to calculate the uncertainty of $\sigma_{N_{qp}}$ in order to calculate the uncertainty of F. We use the central limit theorem and base our uncertainties off the confidence intervals of the standard deviation and the mean, which according to Krishnamoorthy [26], is defined as:

$$\delta\langle x \rangle = |z_{\alpha/2}| \frac{\sigma_x}{\sqrt{N_{photon}}} \tag{4.1}$$

with N_{photon} the number of simulated photons. Also

$$\delta\sigma^2_{N_{qp}} = |z_{\alpha/2}| \frac{\sqrt{2}\sigma^2_{N_{qp}}}{\sqrt{N_{photon}}} \tag{4.2}$$

with $|z_{\alpha/2}| = 1.96$ the standard normal quantity for a 95% confidence interval.

Using $F = \frac{\sigma^2_{N_{qp}}}{\langle N_{qp} \rangle}$ and quadratically summing the uncertainties we obtain:

$$\delta F = \delta \left(\frac{\sigma^2_{qp}}{\langle N_{qp} \rangle} \right) = \sqrt{\left(\frac{\delta\sigma^2}{\langle N_{qp} \rangle} \right)^2 + \left(\frac{\sigma^2}{\langle N_{qp} \rangle^2} \delta\langle N_{qp} \rangle^2 \right)^2} \tag{4.3}$$

Which simplifies to:

$$\delta F = |z_{\alpha/2}| \sqrt{2 + \frac{\sigma^2_{qp}}{\langle N_{qp} \rangle^2}} \frac{F}{\sqrt{N_{photon}}} \approx |z_{\alpha/2}| \sqrt{2} \frac{F}{\sqrt{N_{photon}}} \tag{4.4}$$

since $\frac{\sigma^2_{N_{qp}}}{\langle N_{qp} \rangle^2} << 2$. The result in equation 4.4 gives the uncertainty in the determined Fano factors. Equation 4.1 is used for the uncertainties on all mean quantities: $\langle N_{qp} \rangle$, η and $\langle E \rangle$. To check if this uncertainty is satisfactory, we investigate the variance in the Fano factor at around 10^4 photons. Figure 4.2 shows the Fano factor as a function of the number of simulated photons, along with upper and lower bounds of the uncertainty given by equation 4.4. We see that the oscillation in F due to statistical fluctuations stays well within the bounds set by the uncertainties.

Other sources of error

The error due to the chosen stepsize is considered smaller than the derived uncertainty, as figure 3.11 shows that the Fano factor does not converge for smaller stepsizes. The error due to numerical uncertainties in the values in table 3.1 is also neglected, as we will show that these values have no effect on the Fano factor (section 4.1.3). Therefore, we conclude that equations 4.1 and 4.4 describe the uncertainties in the simulation results well.

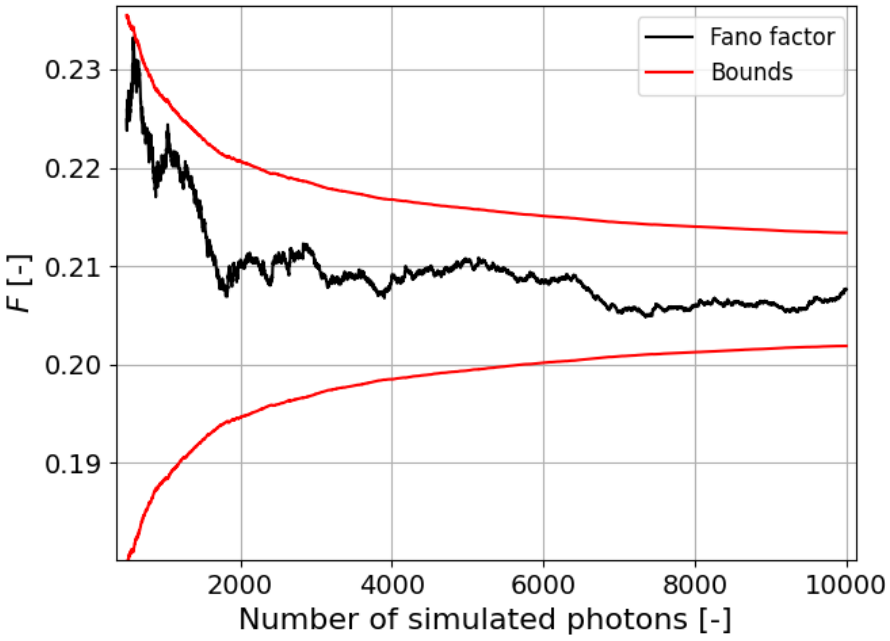

Figure 4.2: The Fano factor as a function of the number of simulated photons used to calculate the Fano factor (black), along with the upper and lower bound of the uncertainty in F calculated from equation 4.4 (red). The bounds are added/subtracted to/from the value of F after 10000 photon simulations. This figure illustrates that the uncertainties calculated the Fano factor suffice.

4.1.3. Materials

To test the dependency of the Fano factor on material properties, simulations were performed for 3 different metals. Figures 4.3, 4.4 and 4.5 show the number of excess quasiparticles N_{qp} due to a photon with energy Q, using the material parameters for tin, niobium and aluminium respectively (see table 3.1). These materials were chosen because the first two appear in similar research performed by Kurakado [18] and by Rando et al. [11] and are used in their simulations. The latter, aluminium, is used because this metal is used in MKIDs that are Fano-limited.

Each simulation consisted of 10^4 individual photon simulations. A photon energy of $Q = 5.75$ eV (= $10^4\Delta_{Sn}$) was used for the Sn and Nb simulations. To save calculation time, the incident photon energy for aluminium was reduced by a factor 10, leading to the creation of less quasiparticles per simulated photon. The gap energy Δ of aluminium is lower than the gap energies of tin and niobium. Because the calculations are performed in units of Δ, metals with lower gap energies and higher Debye energies take more time to simulate since there are more bins needed to descretize these materials. Section 4.1.4 will show that the incident photon energy Q holds no relation to the Fano factor, so this decision has no effect on F.

The Fano factors found for these parameters are $F = 0.206 \pm 0.006$, $F = 0.208 \pm 0.006$ and $F = 0.210 \pm 0.006$ for tin, niobium and aluminium respectively. The values for tin and niobium are in agreement with the values found in earlier research, $F = 0.195 \pm 0.01$ and $F = 0.22 \pm 0.01$ for tin [18] and niobium respectively [11]. The found values have overlap with their uncertainties, we therefore conclude that the Fano factor is independent of material and has a value of $F = 0.208 \pm 0.003$.

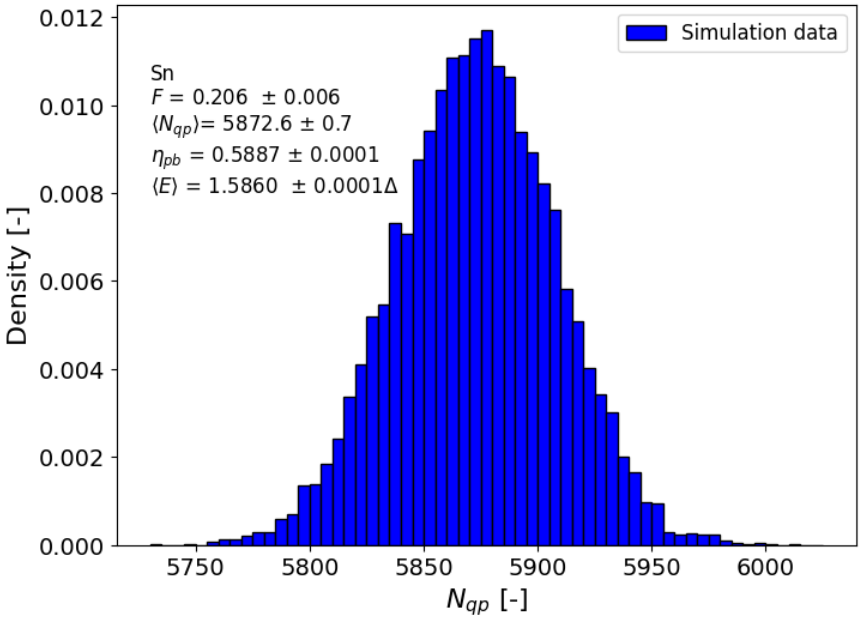

Figure 4.3: Results of the simulation using Sn as a superconductor. The figure shows the spread in the number of generated quasiparticles N_{qp} due to a single photon ($Q = 5.75$ eV). 10^4 photons were simulated. Bin size of 5 quasiparticles. Left upper corner, from top to bottom: Simulated material, Fano factor, mean number of generated quasiparticles, pair breaking efficiency, mean quasiparticle energy.

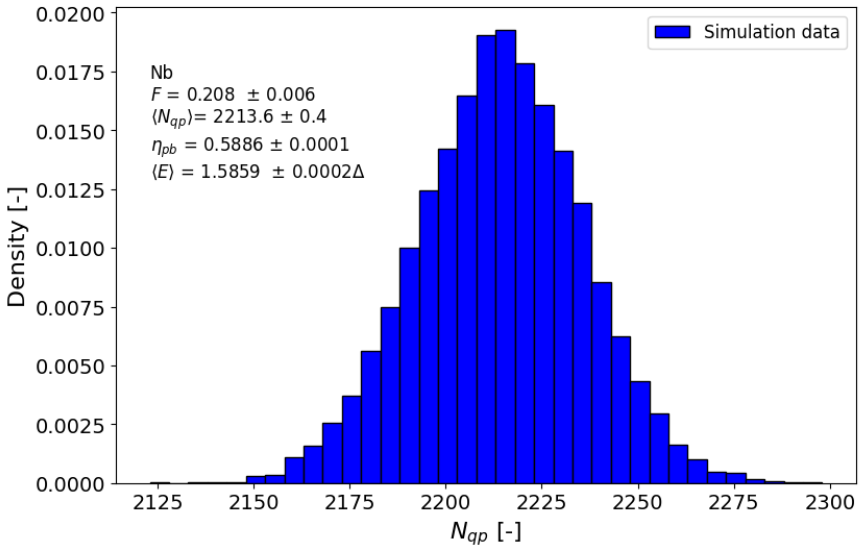

Figure 4.4: Results of the simulation using Nb as a superconductor. The figure shows the spread in the number of generated quasiparticles N_{qp} due to a single photon ($Q = 5.75$ eV). 10^4 photons were simulated. Bin size of 5 quasiparticles.Left upper corner, from top to bottom: Simulated material, Fano factor, mean number of generated quasiparticles, pair breaking efficiency, mean quasiparticle energy.

4.1.4. Photon energy

To test if the Fano factor is influenced by the energy of the photon that hits the detector, photons were simulated at different photon energies Q (ranging from $10^3\Delta$ to $10^4\Delta$, with 10^4 photons simulated per energy level). The results are shown in figures 4.6 and 4.7. The relation between $\langle N_{qp} \rangle$ and Q shown

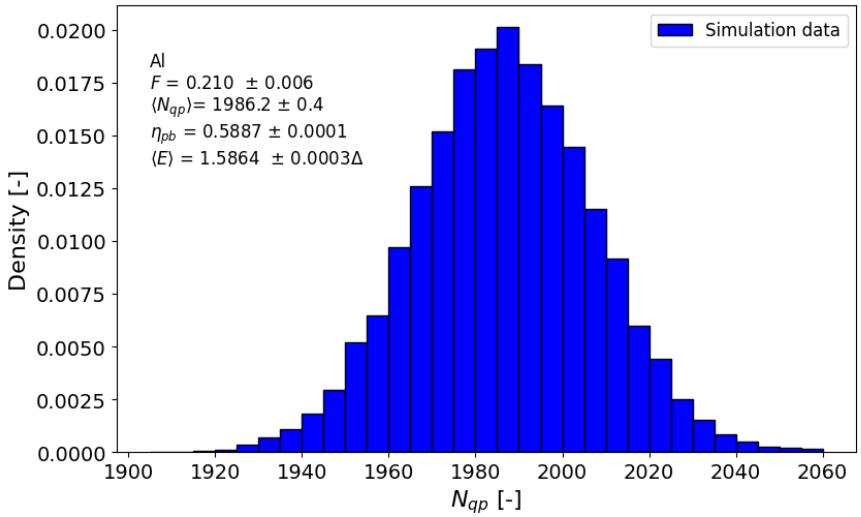

Figure 4.5: Results of the simulation using Al as a superconductor. The figure shows the spread in the number of generated quasiparticles N_{qp} due to a single photon ($Q = 0.575$ eV). Note that the photon energy is a factor 10 lower compared to figures 4.3 and 4.4. 10^4 photons were simulated. Bin size of 5 quasiparticles. Left upper corner, from top to bottom: Simulated material, Fano factor, mean number of generated quasiparticles, pair breaking efficiency, mean quasiparticle energy.

in figure 4.6 is linear. This is expected, as higher Q allows for the creation of more quasiparticles, but does not change the distributions describing the interactions between the quasiparticles and phonons. Figure 4.7 shows the Fano factor as a function of the photon energy. The Fano factor remains constant for increasing Q. We conclude that the photon energy has no effect on the Fano factor. We keep our earlier result that $F = 0.208 \pm 0.003$. Keep in mind that higher photon energies do improve the resolution of an MKID according to equation 2.6.

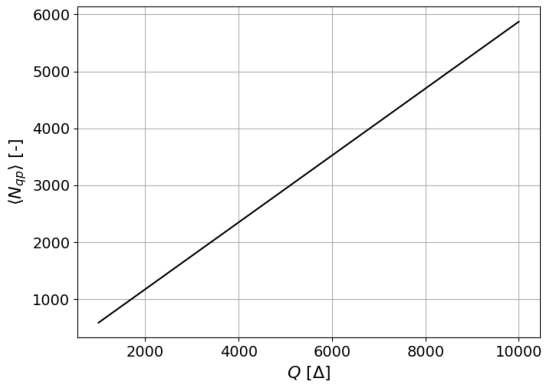

Figure 4.6: Number of quasiparticles $\langle N_{qp} \rangle$ as a function of the energy Q of the incoming photon. The error bars in the Fano factor were calculated according to equation 4.4. As one expects, the relation is linear as a higher energy photon means there is more energy available for the creation of quasiparticles (Sn, 200 Δ^{-1} stepsize).

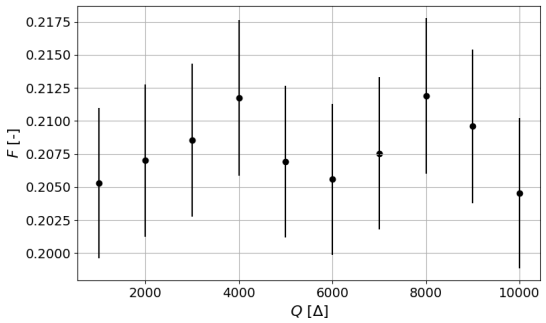

Figure 4.7: F as a function of the energy Q of the incoming photons with 10000 simulated photons per photon energy (Sn, 200 Δ^{-1} stepsize). The error bars were calculated according to equation 4.4.

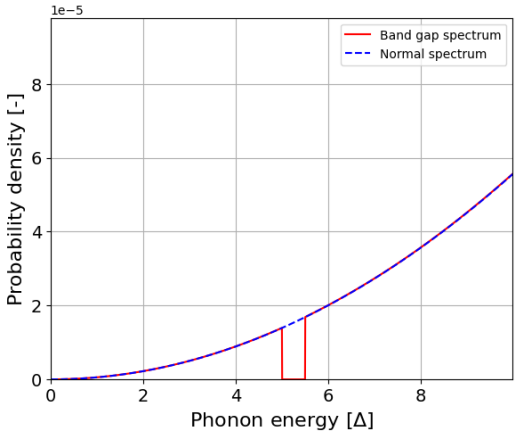

Figure 4.8: Example of a phonon spectrum with a band gap (blue), along with the normal Debye spectrum (red). In this case, phonon energies from 5 to 5.5Δ are prohibited in the Debye phonon spectrum.

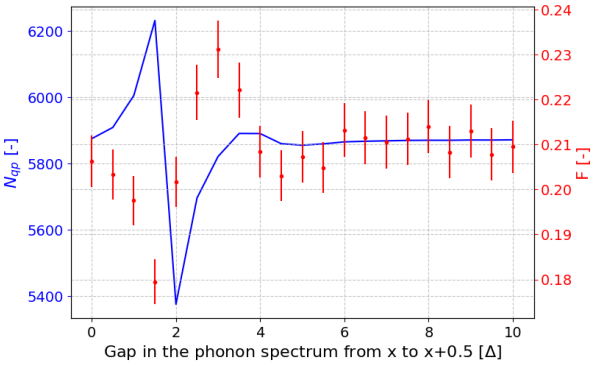

Figure 4.9: Number of quasiparticles $\langle N_{qp} \rangle$ and F as a function of the phonon energies blocked by the simulated phonon bandgap. Each data point has 10^3 simulated photons. Each filter has a width of 0.5Δ (from 0-0.5Δ, 0.5-1Δ, 1.0-1.5Δ etc.).

4.1.5. Tuning the phonon spectrum

Because the choice of materials and the photon energy have no effect on the Fano factor, the only variable left to test is the phonon spectrum. Whether or not tuning the phonon spectrum is realistically achievable will be discussed in section 4.2.4, but for this section we will assume we can alter the allowed phonon energies in any material at will.

In a fictional ideal pair breaking detector, the only available phonon energy should be $\Omega = 2\Delta$. In that case, phonons only create quasiparticles with $E = \Delta$ (since it is the only allowed outcome when a phonon with $\Omega = 2\Delta$ breaks a pair), achieving η_{pb} = 1 and $F = 0$. The reasoning behind this is that a photon with a certain energy Q now always produces the same N_{qp}, meaning σ_{qp} in equation 2.10 becomes 0, resulting in $F = 0$.This example of an ideal MKID is not physically accurate, as it initialises all phonons at energy 2Δ in the simulation and skips the entire down-conversion process. It does serve as a useful thought experiment to better understand the effects of band gaps in the phonon spectrum.

If we want to increase η_{pb} to produce more quasiparticles per incoming photon, the amount of "wasted" energy needs to be decreased. Here wasted energy means energy that is not directly used to create quasiparticles. This is the energy stored in unproductive phonons ($0 < \Omega < 2\Delta$) and the energy above Δ stored in quasiparticles ($\Delta < E < 3\Delta$), meaning a $E = 2\Delta$ quasiparticle "wastes" Δ energy. The total energy that is "wasted" in this way accounts for the 41% energy missing from η_{pb} in the results shown above.

The amount of wasted energy can be reduced by introducing band gaps in $\alpha^2(\Omega)F(\Omega)$ (see figure 4.8). These band gaps prohibit phonons of certain energies from being created. This concerns the initially created phonons at the start of a simulation (see equation 3.1 and figure 3.4), as well as the phonons emitted by a quasiparticle (see equation 3.3 and figure 3.7). To test how the Fano factor reacts on phonon band gaps, we block out different energy levels at different energy levels and perform simulations with these customised phonon spectrum to observe the effect.

Figure 4.9 show the results from introducing band gaps of width Δ in $\alpha^2(\Omega)F(\Omega)$ at different energies. 10^4 photons were simulated per band gap and the band gaps range from 0-0.5 Δ to 10-10.5 Δ. We can see that around 6Δ the band gaps no longer influence the Fano factor. We can also see that blocking low energy phonons from 0-2Δ has the most positive impact on the Fano factor. A phonon band gap from 0-2Δ should yield a lower Fano factor. Therefore, a 0-2Δ band gap is simulated.

Figure 4.10 shows the results from simulating a 0-2Δ phonon band gap. Using this band gap, the Fano factor improves from $F = 0.208 \pm 0.003$ to $F = 0.151 \pm 0.004$, which is an improvement of 27%. The pair breaking efficiency also improves from $\eta_{pb} = 0.5887 \pm 0.0001$ to $\eta_{pb} = 0.6648 \pm 0.0001$, which is

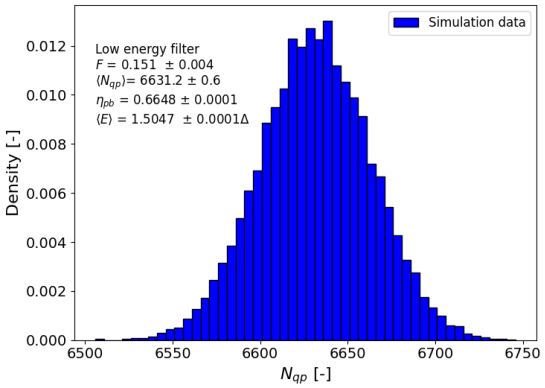

Figure 4.10: Results when using a 0-2Δ phonon band gap in Sn for 10^4 photons. The Fano factor is reduced by 27% compared to the results without a phonon band gap.

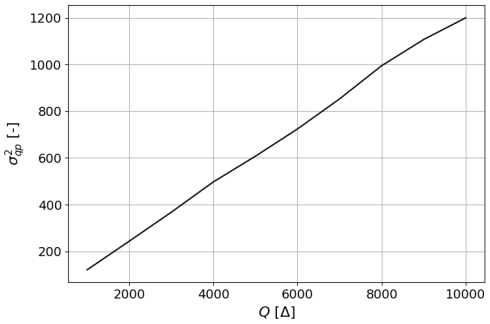

Figure 4.11: σ_{qp}^2 as a function of Q. We can see that σ_{qp}^2 scales linearly like $\langle N_{qp} \rangle$ in figure 4.6, explaining why the Fano factor remains constant with increasing Q.

an improvement of 13%. If we take $J = 0$ for the phonon loss factor, using equation 2.6 we obtain $R_{filt}/R_{norm} = 1.24$, with R_{filt} the resolving power with the 0-2Δ band gap and R_{norm} is the resolving power of an unaltered MKID. This means that with the 0-2Δ band gap, the resolving power of an MKID would improve with 24%. The contributions of the improvements of F and η_{pb} are 17% and 6% respectively. Section 4.1.5 discusses the possibility of band gap in a real metal.

4.2. Discussion

4.2.1. Simulation improvements

There are some ways the accuracy of the simulation could be improved. By taking an even smaller step sizes the accuracy of the simulation improves, although computation times would get longer. This latter issue could be resolved by running parallel calculations on multiple computers, or even on the same computer with multiple cores. This is possible because all photon simulations are independent. The fano factor would not be influenced as we can see in figure 3.11, but other constants like η_{pb} could be determined even more accurately.

A second improvement could be to model phonon loss to the environment, although as mentioned before, we do not do this because we are modeling for Fano-limited MKIDs ($J = 0$).

Thirdly, the first steps of the down-conversion process shown in figure 2.11 could be modeled. In this simulation, we initialize a group of phonons in a range of energies according to equation 3.1, the sum of which equals the photon energy Q. In reality, the incident photon breaks a single Cooper pair that starts to send out phonons that break more Cooper pairs, which can in turn send out more phonons. This continues until the down-conversion process is complete [19]. Although it probably would have little effect on the outcome, modeling these first steps would make the simulation more physically accurate.

Lastly, one could opt to model other interactions in the simulation. We would then need to take into account multiple interactions for the same particle. Instead of assuming that a quasiparticle, for example, emits a phonon no matter what, we would also need to randomly choose between whether the quasiparticle emits a phonon or recombines into a cooper pair. This extra step would be required for all interactions, increasing the computing times. As shown in section 3.2, these other interactions would not have big impacts on the outcomes of the simulation. Therefore, the only relevant improvement that could be made would be smaller stepsize of the simulation while using parallel computing. This would not have an impact on our result for F.

4.2.2. The Fano factor as a constant

The results from sections 4.1.3 and 4.1.4 show that the Fano factor neither depends on the choice of superconductor material or the energy of the incoming photons.

The independence of F on the radiation energy Q can be explained if we realize that a higher mean number of generated quasiparticles also means that more paths are available for the down-conversion process. This increase means $\sigma^2_{N_{qp}}$ increases, as we get a wider spread in N_{qp}. Apparently $\sigma^2_{N_{qp}}$ scales relative to N_{qp}. Figure 4.11 shows that this is indeed the case. The same concept can be applied to the choice of material. Lower Δ essentially means more quasiparticles can be created with the same photon energy, but the spread in the possible outcomes also increases. Therefore, the choice of material does not influence F. Lower Δ would still improve the sensitivity of the MKID through equation 2.6.

4.2.3. Pair breaking efficiency and the Fano factor

The Fano factor seems to share a relation with the pair breaking efficiency η_{pb} when altering the phonon spectrum. Higher pair breaking efficiency seems to go hand in hand with a lower Fano factor. This seems logical as a higher mean pair breaking efficiency means higher mean N_{qp}, reducing the Fano factor. Higher η_{pb} also positively impacts the resolving power as seen in equation 2.6, adding an additional gain of 6% to the sensitivity of the MKID.

4.2.4. Tuning the phonon spectrum of real materials

The improvement in the Fano factor shown in figures 4.9 and 4.10 is the only improvement of the Fano factor that was found with this research. The question remains if we can create a band gap in the phonon density of states from 0-2Δ, similar to the one shown in figure 4.8. This would improve the Fano factor and the pair breaking efficiency, resulting in an increase in the resolving power of the MKID.

The engineering of phonon spectra in materials is a practice that is known within the scientific community [4][27][28][29] and has even been used to improve phonon trapping in MKIDs [4]. A band gap can be created by altering the geometry of a material, like in figure 4.12. By introducing holes with a specific spacing and shape, a range of phonon energies can be blocked. The specific geometry of these holes needs to be calculated [27][28][29]. By introducing the holes, the the lattice constant a of the material is altered. The appearance of a band gap can be explained if we view the phonons as particles [30] and their "size" defined by their wavelength λ. If we want to block phonons with λ size, we need holes with approximately the same size, so the phonons can not pass in between the holes. Larger (lower energy) phonons are large enough to ignore the holes completely and smaller (higher energy) phonons can pass in between the holes. This produces a band gap around λ with a certain width [28]. Because we want to block phonons from 0-2Δ, we will approximate the lattice constant for a band gap around a central energy $\Omega = \Delta$.

A rough estimate of the lattice constant for a 0-2 Δ band gap can then be made with

$$a \approx \lambda_{phonon} = \frac{\langle v_{Al} \rangle}{f_{phonon}}, \tag{4.5}$$

with $\langle v_{Al} \rangle$ the average speed of sound in aluminium and f_c the frequency of the band gap [31]. If we take $f_c = \frac{\Delta_{Al}}{h} = 41$ GHz, with $\Delta_{Al} = 0.17meV$ (see table 3.1) and $h = 4.13610^{15}$ eV·s. We obtain

$$a \approx \frac{\langle v_{Al} \rangle h}{\Delta_{Al}}. \tag{4.6}$$

$\langle v_{Al} \rangle$ is given by [32]:

$$\frac{1}{\langle v^3_{Al} \rangle} = \frac{1}{3}\left[\frac{1}{v^3_L} + \frac{2}{v^3_T}\right], \tag{4.7}$$

with $v^3_L = 6650$ m/s and $v^3_T = 3260$ m/s the longitudinal and transverse mode speeds in aluminium respectively [33]. Using equations 4.6 and 4.7 we get $\langle v_{Al} \rangle = 3360$ m/s and $a_{BG} \approx 80$ nm. The feature sizes of the inductor on MKIDs are about 1-10 um [17], so holes around the size of a_{BG} could, in theory,

be implemented to create a phonon band gap. The smallest feature size would be around 40 nm, since the holes are smaller than the lattice constant (see figure 4.12). This feature size is achievable with current lithography technologies [27]. Further research is needed to calculate the exact size and shape of the holes needed to create such a band gap. This research should take into account all possible phonon modes.

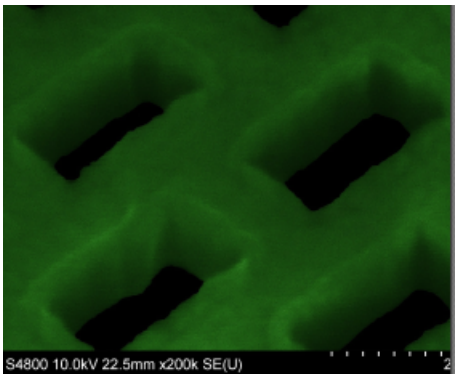

Figure 4.12: Holes in the SiN surrounding the inductor of an MKID to prevent phonon escape. The smalles feature is the short side of the rectangular holes, which is about half the total length of a cell. Figure from Ref. [4].

Creating a perfect band gap between 0-2Δ (0 - 82 GHz) would improve the resolving power of the MKID with 24%, with a 13% improvement in η_{pb} and a 27% improvement in F. This is assuming the band gap is perfect and all other specifications of the MKID remain the same. In reality the improvement would probably be a lot lower, because the band width of these band gaps is typically 10-20% around the energy it is designed for [27][29]. A 0-2Δ gap would need a 200% band width around Δ. Acknowledging this restriction, blocking phonons close to 2Δ should be prioritised over blocking low energy phonons, as the first group has more effect on the Fano factor than the latter (see figure 4.9). It is also important that our real band gap is very exact, as blocking phonons just above 2Δ would result in a decrease in both $\langle N_{qp} \rangle$ and η_{pb}, as well as an increase in F (see figure 4.9). This would reduce the resolving power.

Further research is needed to prove whether or not creating a phonon band gap in the inductor of an MKID is beneficial or not, starting by making calculations for the band gaps that are required. Another way of improving the resolving power of an MKID would be to use a superconductor with a lower T_c as these materials have lower Δ. To get the same maximum increase in the resolving power as from the introduction of a band gap, a superconductor with critical temperature at least 35% lower than aluminium ($T_c = 1.2$ K) would be needed. This would be impractical as these types of MKIDs would require even lower working temperatures, while current MKIDs already operate at $T \approx 100$ mK. Therefore, efforts should be made to test the viability of a phonon band gap in an MKID to improve its resolving power.

5

Conclusion

The aim of this report was to investigate if and how the Fano factor for single-photon absorption in the superconductor of an MKID could realistically be improved. To answer this question, a Monte Carlo simulation simulating incoming photons on a superconducting piece of metal was created. The simulation uses discretized energies to efficiently calculate the outcomes of phonon and quasiparticle interactions based on their probability distributions. The only interactions that were modeled are Cooper pair breaking by phonons and the emission of phonons by quasiparticles. The rest of the interactions, such as phonon scattering and quasiparticle recombination, could be neglected due to their long lifetimes. The simulation was validated by showing that the mean number of generated quasiparticles $\langle N_{qp} \rangle$ and the mean quasiparticle energy $\langle E \rangle$ converge for decreasing stepsize, and that F is not influenced by the stepsize used in the simulation. A series of tests was performed to show that the Fano factor does not depend on the superconducting material used in the MKID. The Fano factor is also independent of the energy of the incident photon and has value of $F = 0.208 \pm 0.003$, which agrees with previous results. The Fano factor F can be improved with up to 27%, to $F = 0.151 \pm 0.004$, by introducing a band gap from 0-2 Δ in the phonon spectrum. The pair breaking efficiency η_{pb}, the measure for the amount of photon energy that is efficiently used to create Cooper pairs, also improves from $\eta_{pb} = 0.5887 \pm 0.0001$ to $\eta_{pb} = 0.6648 \pm 0.0001$ when using this band gap. This is an improvement of 13%. This results in a total improvement of 24% for the resolving power R of an MKID, assuming no phonons are lost to the environment ($J = 0$). Using a superconductor with lower Δ to improve R with the same amount be impractical, because it requires a 35% lower working temperature for the MKID, while the current working temperature is already about 100 mK. We conclude that it would be beneficial to implement a phonon band gap from 0-2Δ to improve the resolving power of an MKID.

Phonon band gaps are a known phenomenon within science. Periodic holes in a crystal lattice can block certain phonon energies. A band gap in the phonon spectrum of aluminium from 0-2Δ would require a lattice constant a of approximately 80 nm, which would be possible because the aluminium inductor in MKIDs has features of in the order of 1 um. The smallest feature size would then be approximately 40 nm, which is achievable with current technology. The real improvement by implementation of a band gap would probably be a lot less than 24%, due to the limitations of these band gaps. Further research is needed to determine whether or not it is possible to create a viable band gap without sacrificing other properties of the MKID.

References

[1] NASA et al. *Artist impression of WASP-39 b and its star*. 2022. URL: https://www.esa.int/ESA_Multimedia/Images/2022/08/Artist_impression_of_WASP-39_b_and_its_star (visited on 12/01/2024).

[2] NASA. *Webb key facts*. URL: https://webb.nasa.gov/content/about/faqs/facts.html (visited on 11/01/2024).

[3] NASA, JPL-Caltech, and L.B. De La Torre. *Spectroscopy infographic - Exoplanet Exploration: Planets beyond our Solar System*. URL: https://exoplanets.nasa.gov/resources/2270/spectroscopy-infographic/ (visited on 11/01/2024).

[4] Pieter de Visser et al. "Fano-dominated energy resolution at visible- near-infrared wavelengths in MKIDs". From a presentation presented at the international conference on Low Temperature Detectors, Deajeon, South Korea. 2023.

[5] Kevin Kouwenhoven et al. "Resolving Power of Visible-To-Near-Infrared Hybrid $\beta-\mathrm{Ta/Nb-Ti-N}$ Kinetic Inductance Detectors". In: *Phys. Rev. Appl.* 19 (3 Mar. 2023), p. 034007. DOI: 10.1103/PhysRevApplied.19.034007. URL: https://link.aps.org/doi/10.1103/PhysRevApplied.19.034007.

[6] Peter Day et al. "A broadband superconducting detector suitable for use in large arrays". In: *Nature* 425.6960 (Oct. 2003), pp. 817–821. DOI: 10.1038/nature02037. URL: https://doi.org/10.1038/nature02037.

[7] J. R. Hook and H. E. Hall. "Crystal Dynamics". In: *Solid State Physics*. 2nd ed. John Wiley & Sons, Sept. 1991, pp. 33–74.

[8] Ioannis Papadimitriou, Claire Utton, and Panos Tsakiropoulos. "Ab Initio Study of Ternary W5Si3 Type TM5Sn2X Compounds (TM = Nb, Ti and X = Al, Si)". In: *Materials* 12.19 (2019). ISSN: 1996-1944. DOI: 10.3390/ma12193217. URL: https://www.mdpi.com/1996-1944/12/19/3217.

[9] S. B. Kaplan et al. "Quasiparticle and phonon lifetimes in superconductors". In: *Phys. Rev. B* 14 (11 Dec. 1976), pp. 4854–4873. DOI: 10.1103/PhysRevB.14.4854. URL: https://link.aps.org/doi/10.1103/PhysRevB.14.4854.

[10] Steven H. Simon. *The Oxford Solid State Basics*. Oxford University Press, June 2013.

[11] N. Rando et al. "The properties of niobium superconducting tunneling junctions as X-ray detectors". In: *Nuclear Instruments and Methods in Physics Research Section A: Accelerators, Spectrometers, Detectors and Associated Equipment* 313.1 (1992), pp. 173–195. ISSN: 0168-9002. DOI: https://doi.org/10.1016/0168-9002(92)90095-L. URL: https://www.sciencedirect.com/science/article/pii/016890029290095L.

[12] J. R. Hook and H. E. Hall. "Superconductivity". In: *Solid State Physics*. 2nd ed. John Wiley & Sons, Sept. 1991, pp. 278–313.

[13] Gerd Czycholl. "Superconductivity". In: *Solid State Theory, Volume 2: Applications: Non-equilibrium, Behavior in External Fields, Collective Phenomena*. Berlin, Heidelberg: Springer Berlin Heidelberg, 2023, pp. 197–251. ISBN: 978-3-662-66963-1. DOI: 10.1007/978-3-662-66963-1_5. URL: https://doi.org/10.1007/978-3-662-66963-1_5.

[14] E. Zubov. "Proximity effect and self-consistent field in a normal metal-superconductor structure". preprint. Mar. 2019. URL: https://www.researchgate.net/publication/331731248_Proximity_effect_and_self-consistent_field_in_a_normal_metal-superconductor_structure.

[15] Jiachen Gao et al. "Equivalence of the Effects on the Complex Conductivity of Superconductor due to Temperature Change and External Pair Breaking". In: *Journal of Low Temperature Physics* 151 (Apr. 2008). DOI: 10.1007/s10909-007-9688-z.

[16] Pieter De Visser. “Quasiparticle dynamics in aluminium superconducting microwave resonators”. PhD thesis. Tu Delft, 2014.

[17] Pieter J De Visser et al. “Phonon-trapping-enhanced energy resolution in superconducting single-photon detectors”. In: *Physical Review Applied* 16.3 (2021), p. 034051.

[18] M. Kurakado. “Possibility of high resolution detectors using superconducting tunnel junctions”. In: *Nuclear Instruments and Methods in Physics Research* 196.1 (1982), pp. 275–277. ISSN: 0167-5087. DOI: https://doi.org/10.1016/0029-554X(82)90654-1. URL: https://www.sciencedirect.com/science/article/pii/0029554X82906541.

[19] A. G. Kozorezov et al. “Quasiparticle-phonon downconversion in nonequilibrium superconductors”. In: *Phys. Rev. B* 61 (17 May 2000), pp. 11807–11819. DOI: 10.1103/PhysRevB.61.11807. URL: https://link.aps.org/doi/10.1103/PhysRevB.61.11807.

[20] U. Fano. “Ionization Yield of Radiations. II. The Fluctuations of the Number of Ions”. In: *Phys. Rev.* 72 (1 July 1947), pp. 26–29. DOI: 10.1103/PhysRev.72.26. URL: https://link.aps.org/doi/10.1103/PhysRev.72.26.

[21] Nicholas Zobrist et al. “Membraneless Phonon Trapping and Resolution Enhancement in Optical Microwave Kinetic Inductance Detectors”. In: *Phys. Rev. Lett.* 129 (1 July 2022), p. 017701. DOI: 10.1103/PhysRevLett.129.017701. URL: https://link.aps.org/doi/10.1103/PhysRevLett.129.017701.

[22] A. M. Johansen. “Monte carlo methods”. In: *International Encyclopedia of Education* (2010), pp. 296–303. DOI: 10.1016/b978-0-08-044894-7.01543-8.

[23] W. L. McMillan and J. M. Rowell. “Tunneling and strong-coupling superconductivity”. In: *Superconductivity* (2018), pp. 561–613. DOI: 10.1201/9780203737965-11.

[24] Charles Kittel. *Introduction to Solid State Physics*. Wiley, Nov. 2004.

[25] G. R. Stewart. “Measurement of low-temperature specific heat”. In: *Review of Scientific Instruments* 54 (1 1983), pp. 1–11. DOI: 10.1063/1.1137207.

[26] Kalimuthu Krishnamoorthy. *Handbook of Statistical Distributions with Applications*. Chapman and Hall/CRC, June 2006, pp. 130–133.

[27] T. Puurtinen et al. “A composite phononic crystal design for quasiparticle lifetime enhancement in kinetic inductance detectors”. In: *Journal of Low Temperature Physics* 199 (3-4 2020), pp. 577–584. DOI: 10.1007/s10909-020-02423-4.

[28] M. S. Kushwaha et al. “Acoustic band structure of periodic elastic composites”. In: *Phys. Rev. Lett.* 71 (13 Sept. 1993), pp. 2022–2025. DOI: 10.1103/PhysRevLett.71.2022. URL: https://link.aps.org/doi/10.1103/PhysRevLett.71.2022.

[29] Nobuyuki Zen et al. “Engineering thermal conductance using a two-dimensional phononic crystal”. In: *Nature Communications* 5.1 (Mar. 2014). DOI: 10.1038/ncomms4435. URL: https://doi.org/10.1038/ncomms4435.

[30] D.L. Chandler. *Explained: Phonons*. July 2010. URL: https://news.mit.edu/2010/explained-phonons-0706 (visited on 09/01/2024).

[31] Dr. A. Akhmerov. private communication. Email about the implementation of phonon band gaps in a real material. 2023.

[32] A.H. Harker. *Phonon heat capacity*. Lecture given at University College London. URL: https://www.ucl.ac.uk/~ucapahh/teaching/3C25/Lecture10s.pdf.

[33] S.B. Kaplan. “Acoustic matching of superconducting films to substrates”. In: *Journal of Low Temperature Physics* 37.3-4 (Nov. 1979), pp. 343–365. DOI: 10.1007/bf00119193. URL: https://doi.org/10.1007/bf00119193.